ANL/DIS-14/12

Argonne Below Ground Model Part I: Transport and Dispersion in Underground Transportation Systems

Decision and Information Sciences Division

About Argonne National Laboratory
Argonne is a U.S. Department of Energy laboratory managed by UChicago Argonne, LLC under contract DE-AC02-06CH11357. The Laboratory's main facility is outside Chicago, at 9700 South Cass Avenue, Argonne, Illinois 60439. For information about Argonne and its pioneering science and technology programs, see www.anl.gov.

ANL/DIS-14/12

Argonne Below Ground Model Part I: Transport and Dispersion in Underground Transportation Systems

by
D.F. Brown and J.C. Liljegren
Decision and Information Sciences Division
Argonne National Laboratory

August 2014

Contents

Figures

Figures (Cont.)

Tables

Nomenclature

Acronyms

BGM	Below Ground Model
c/c	cut and cover
CFL	Courant-Fredrichs-Levy
GB	Sarin
GSD	Geometric Standard Deviation
HVAC	Heating, Ventilating, and Air Conditioning
MERV	Minimum Efficiency Reporting Value
NYC	New York City
OP	Organophosphate
SES	Subway Environmental Simulation

Notation

A	cross-sectional area
A_s	surface area
C	mean airborne mass concentration
c'	turbulent concentration fluctuation
C_D	drag coefficient
D	diameter
D_H	hydraulic diameter
d	train hydraulic diameter
f	Darcy-Weisbach friction factor
f_v	flow split: ratio of flow through a vent shaft to the flow through the tunnel
f_{open}	fraction open area between paired tunnel segments of opposite flow direction
g	gravitational acceleration
h_f	loss of mechanical energy per unit mass due to friction
h_r	loss of mechanical energy per unit mass due to form drag
K	mechanical energy loss coefficient; also eddy diffusion coefficient
Kn	Knudsen number
k	surface roughness element height; also diffusion coefficient surface to substrate
L	tunnel segment length
l	train length
m	mass
	P pressure
Pr	Prandtl number
P_∞	atmospheric pressure
Q	volumetric flow rate
Re	tunnel Reynolds number = $D_H U/\nu$
r	surface roughness = k/D_H

S	source or sink of material (mass per volume per time)
Sc	Schmidt number
T	absolute temperature
t	time
U	mean airflow velocity
u'	turbulent airflow fluctuation
u_*	friction velocity
V	train velocity
V_d	deposition velocity
$\tilde{V}$	volume
x	position along a tunnel or train tracks
Z	elevation
β	ratio of airflow velocity induced by a train to actual train velocity; also coefficient of thermal expansion, Appendix B
λ	rate constant for adsorption/desorption; also mean free path
μ	dynamic viscosity of air
ν	kinematic viscosity of air = μ/ρ
ρ	density of air
σ	ratio of train cross-sectional area to tunnel cross-sectional area

1 Introduction

1.1 Background

On March 20, 1995, members of the Japanese cult Aum Shinrikyo released the nerve agent sarin onboard trains in the Tokyo subway, killing 12 people and injuring many more (Smithson and Levy 2000). Although evidence of the vulnerability of subways to a biological attack had existed for decades (U.S. Army 1966), the Tokyo attack focused public attention for the first time on the potential threat posed by chemical and biological agents to millions of daily subway riders. Several successful and unsuccessful attacks on subways around the world since then — combined with the 9/11 attacks in the United States—have further heightened concerns and demonstrated the need for informed response planning and preparation.

The Argonne Below Ground Model (BGM) was developed to provide a comprehensive simulation capability for analysis of subway threats at the level of the entire system. BGM predicts the movement and spread of a chemical or biological agent within an underground subway system, as well as the amount of material released to the environment through station entrances, street-level vents, and tunnel portals. To assess the health consequences of an attack, BGM incorporates a population-effects component in which the movements of each person in the system are independently modeled, thereby allowing their individual exposure, their resulting health end point, and their behavior (in the case of chemical exposure) to be determined.

BGM has been validated against the results of several subway airflow studies. Airflow studies carried out in the Washington, D.C., subway in 2007 and 2008 (Brown et al., unpublished report) and in the Boston subway in 2009, 2010, and 2012 (Brown et al., unpublished report) involved the simultaneous release of multiple gas and particle tracers. In 2013, multiple gas tracers were released in the New York City subway and aboveground (Kalb et al. 2014, unpublished report). Multiple gas and particulate tracers were released in the New York City subway in 2016 (Ervin et al. 2018). In these studies, the time-varying airborne tracer concentrations measured in subway stations throughout the system, as well as onboard selected trains, provided unique datasets for model validation.

Our team has used BGM to conduct a wide range of analyses for many subways. Following are a few of the analyses with associated questions described generically (i.e., without respect to specific subway systems). Table 1 lists key characteristics of all heavy rail subways in the United States and indicates which have been modeled with BGM.

Optimal chemical/biological detector architecture for subway systems. For a specified number of detectors, where should they be located to minimize specified health consequences? For an established architecture, where/how many additional detectors would be necessary to achieve a desired system-wide level of protection? Would detectors located in the subway provide useful indication of an aboveground agent release or a release in an attached transit facility?

Table 1. Characteristics of heavy-rail subway systems in the United States.

City Operating agency	New York NYCT[a]	Washington, D.C. WMATA	Boston MBTA	Philadelphia SEPTA/ PATCO	San Francisco BART
Modeled using BGM?	Yes	Yes	Yes	No	Yes
Belowground lines	25	5	4	3	4
Belowground stations	326	45	27	35	15
Stations with connections to multiple belowground lines	13	3	6	4	0[b]

City Operating agency	Chicago CTA	NJ/NYC PATH	Los Angeles LAMTA	Atlanta MARTA	Baltimore MTA
Modeled using BGM	Yes	Yes	Yes	No	No
Belowground lines	2	3	2	2	1
Belowground stations	18	11	16	9	9
Stations with connections to multiple belowground lines	0[c]	2	1	1	N/A

[a] CTA = Chicago Transit Authority; BART = Bay Area Rapid Transit; LAMTA = Los Angeles Metropolitan Transit Authority; MARTA = Metropolitan Atlanta Rapid Transit Authority; MBTA = Massachusetts Bay Transportation Authority; MTA = Maryland Transit Administration; NYCT = New York City Transit; PATH = Port Authority Trans-Hudson; SEPTA/PATCO = Southeastern Pennsylvania Transportation Authority/Port Authority Transit Corporation; WMATA = Washington Metropolitan Area Transit Authority

[b] Four downtown stations connect to the underground light-rail MUNI system.

[c] Lines are connected through two passageways downtown.

Detector performance. How do the various aspects of detector performance (e.g., sensitivity, response time) contribute to the overall system performance, which also depends on detector configuration (e.g., trigger-confirmer), decision response time, and other factors? Which aspects are most important?

Efficacy of response strategies. How well do proposed strategies to respond to a detector alarm mitigate the consequences (e.g., how many lives are potentially saved)? Are there unintended consequences of the proposed actions?

Combined facility/outdoor/subway detector architecture analysis (in collaboration with other national laboratories). How well would the proposed/existing architecture perform against indoor, outdoor, and subway releases of chemical, biological, and radiological agents? What improved level of protection would additional detectors provide and where should they be located?

Chemical detector cost/performance. For existing commercial off-the-shelf chemical detectors, what is necessary, for a range of chemical warfare agents, to achieve various levels of protection considering the effects of subway patrons' responses (including self-evacuation, incapacitation, etc.) leading to a system shutdown?

Fomite transport by rail transit passengers. Would (aboveground) rail transit passengers who had been subjected to an agent release at a station in one city export that threat to distant cities?

1.2 Model Overview

BGM is comprised of three main components: (1) a model of the time-varying airflow in the subway driven by the train operation described in Section 2, (2) a model of the transport and spread of material by the airflow as well as transport by the train cars described in Section 3, and (3) a model of the subway patrons exposed to the airborne material as they move through the system (Liljegren and Brown 2014). Whereas others (Winkler et al. 2006) implemented these processes separately, in BGM they are integrated to enable the effects both of passenger behavior (self-evacuation) on system operation and passenger transport (via particle deposition/resuspension) on airborne concentrations to be represented.

The core of the subway transport model, described in this report, is a series of algorithms to predict the movement and spread of material within the subway system, the main drivers of which are illustrated in Figure 1.

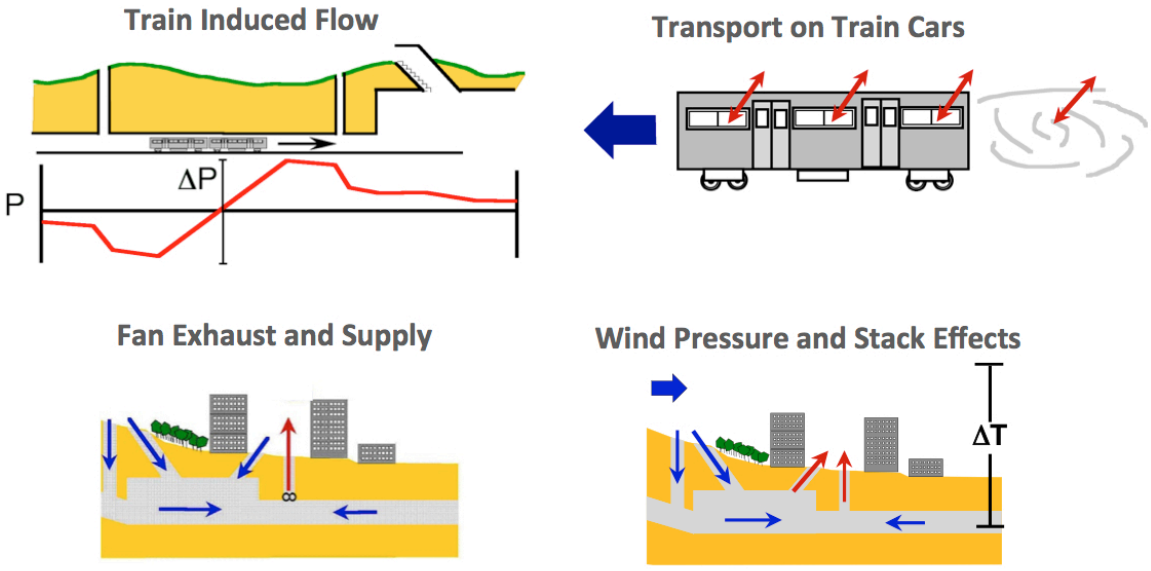

Figure 1. Key drivers for transport and dispersion in subways.

These drivers include:

- Train-induced airflow, often referred to as piston flow, as described in Section 2.1. Piston flow calculations within the subway dispersion model are derived from the Subway Environmental Simulation (SES), a detailed energy load model for subway system design developed in the 1970s (DOT 1976).

- Transport of material by the train cars, as described in Section 3.2. In this case, material is drawn into the train car by the ventilation system in the car, by air leakage, or through open train car doors in stations. The car then acts as a source for this material as it continues through the subway system. Within the model, each train car is represented by a single heating, ventilating, and air conditioning (HVAC) zone with fresh and recirculation ventilation prescribed by the train car specifications and leakage rates that depend on whether doors are open or closed.

- Airflow caused by mechanical ventilation such as under-platform exhaust and emergency fans. These are set within the model according to supply or exhaust rates given by engineering specifications provided by the transit agencies.

- Naturally occurring airflows, that is, temperature-induced "stack" flows or wind pressure-induced flows arising from meteorological conditions. While not calculated directly in the model, these steady-state natural flows can be specified by imposing inflows or outflows at station entrances and vent shafts, as explained in Section 2.2.

In addition to the emission of material from the subway to the aboveground environment, BGM also accounts for the removal of particulate agents by deposition and filtration (Section 4) and the adsorption and desorption of gaseous agents (Section 5). The model accounts for deposition by settling, impaction arising from forced and natural convection in the tunnels, and thermophoretic effects; settling is the dominant mechanism for most biological agents with sizes greater than a few micrometers. Removal of particulate material from fresh and recirculation air streams by the train car filters is accounted for in the train car calculations through an imposed filtration efficiency, which can be treated statistically.

Coupled with the transport model is a population effects model, described in a companion report (Liljegren and Brown 2014), in which the movement of each subway patron in the system is independently modeled and which allows the exposure of these patrons, their resulting health effects, and their responses — in the case of chemical exposure — to be ascertained. The population model has the ability to address vapor adsorption and desorption from the subway patrons, as well as the deposition and resuspension of particles by subway patrons ("fomite transport"). This capability can also be used to assess the amounts of these materials transported beyond the subway by exiting patrons. The population model utilizes average hourly entry and exit counts derived from turnstile data.

Figure 2 presents a schematic illustration of BGM components, inputs, and data flows.

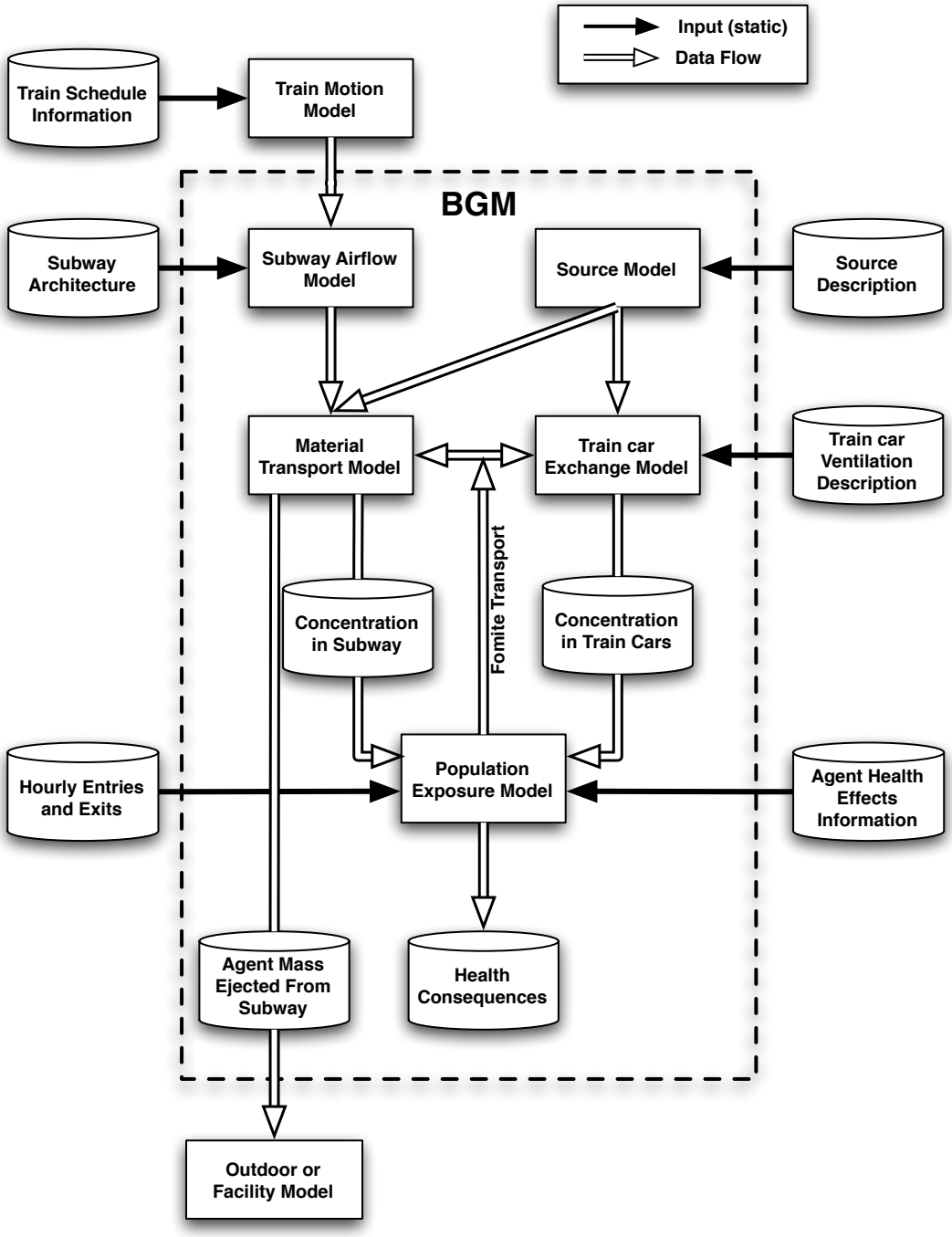

Figure 2. BGM components, inputs, and information flow.

This page intentionally left blank.

2 Subway Airflow

2.1 Airflow by Train Movements

As indicated previously, the calculation of airflow driven by train movements ("*piston flow"*) in BGM is based on the Subway Environmental Simulation (SES) approach (DOT 1976). SES was developed in the 1970s for the purpose of guiding subway ventilation system design under routine and emergency conditions. It comprises four components: (1) a train performance component that determines train acceleration, velocity, position, and heat output from motors, brakes, air conditioning, etc.; (2) an aerodynamic component that uses the train calculations along with descriptions of the geometric arrangement of the system and ventilation equipment to determine the system airflows; (3) a temperature/humidity component that uses the airflows and train heat output to determine the distribution of sensible and latent heat; and (4) a heat sink component that determines the long-term heat input to the surrounding soil through the tunnel walls. SES implements theoretical models bolstered by extensive testing using at-scale test facilities and actual subways to derive subway-specific parameterizations and for validation.

Because SES does not calculate the dispersion of material within the subway, others (Winkler et al. 2006, Coke et al. 2000) have used SES to calculate the airflows and then develop a post-processor program to carry out the material dispersion calculations separately. However, the multiple components of SES combine to create a heavy computational burden that limits the number of scenarios that can be practically simulated. In addition, the SES approach does not allow the actual velocity and position of the trains to be used — elements that BGM can utilize when available. Relying on SES makes extending the modeling framework to previously unconsidered subways a substantial effort and was the consideration that led us to develop a dedicated subway transport and dispersion model that could be easily implemented for any subway, had no limits on size (a critical factor for New York and larger subways), and could utilize real-time train information. To generate the large scenario libraries needed to carry out the subway analyses described earlier, BGM implements only the algorithms comprising the aerodynamic component of SES. In addition to substantially reducing the computational burden, this has the further advantage, described earlier, of enabling the calculations of airflow, material dispersion, and population exposure and dynamics to be interactive. This capability is critical for detection efficacy analyses in which the population response can change the outcome of the simulation such as chemical agents with prompt acute health effects.

2.1.1 Model Description

2.1.1.1 Theoretical Basis

The airflow calculations in BGM, derived from the SES aerodynamic component, represent a one-dimensional, incompressible, turbulent flow model that predicts bulk mean airflow in tunnels, stations, vent shafts, etc. A three-dimensional computational fluid dynamics model of a

complete subway would not only be computationally prohibitive, but is unnecessary for the system-level analyses to be performed.

BGM, following SES, implements the one-dimensional mechanical energy equation, also referred to as the modified Bernoulli equation, that describes the energy balance in a fluid between two points 1 and 2 (Shanes 1962[1]):

$$\left(\frac{P_1}{\rho}+\frac{U_1^2}{2}+gZ_1\right)=\left(\frac{P_2}{\rho}+\frac{U_2^2}{2}+gZ_2\right)+h_f+h_r.$$

P is the static pressure, ρ is the fluid density, $U = Q/A$ is the mean flow velocity equal to the volumetric flow rate Q divided by the cross-sectional area A, $U^2/2$ represents the dynamic pressure per unit mass of fluid; g is gravitational acceleration, and Z is the elevation above some reference datum. The terms h_f and h_r represent, respectively, the loss of mechanical energy per unit mass of fluid due to shear stress at the wall (i.e., friction) and the loss of mechanical energy per unit mass due to form resistance such as bends, changes in area, or other obstacles in the path of the fluid. This equation may be rearranged to express the pressure change ΔP between points 1 and 2 in terms of the change in flow, the change in elevation, and the loss terms:

$$\frac{P_1-P_2}{\rho}=\frac{U_2^2-U_1^2}{2}+g(Z_2-Z_1)+h_f+h_r.$$

In BGM and SES, the subway is represented as a series of connected segments. The cross-sectional area of an individual segment is constant; thus, the segment boundaries denote locations where cross-sectional areas change or where other aspects of the tunnel's or station's geometry markedly change (e.g., single-track to multi-track tunnels, tunnels to stations). For an incompressible fluid, mass continuity requires that the flow velocity U in each segment be constant so that $U_2^2 - U_1^2 = 0$. In addition, the elevation changes in subway tunnels are generally unimportant so that the $g(Z_2 - Z_1)$ term is ignored in SES and BGM. The pressure change in a segment then is solely dependent on the loss terms.

The loss terms are related to the dynamic pressure term $U^2/2$:

$$h_f = f\frac{L}{D}\frac{U^2}{2},$$
$$h_r = K\frac{U^2}{2}.$$

Here, f is the Darcy-Weisbach friction factor, L is the length of the segment (the distance between points 1 and 2), and D is the diameter. Because subway tunnels and vent shafts are rarely circular, the hydraulic diameter D_H is used, which is equal to

$$D_H = \frac{4 \times Cross\ sectional\ area}{Perimeter}.$$

[1] Equation 10-25, page 287.

The loss coefficient *K* is actually the combination of all such loss coefficients for all form resistances in the segment, that is, between points 1 and 2. Friction factors and loss coefficients for the subway are discussed in Section 2.1.2 concerning subway architecture description. It is important to note that *determining the loss coefficients is the most critical step in the airflow calculation in BGM*. As an example, at any time step, losses from many vent shafts or station entrances will affect the flow, and the flows generated from an individual train can have an influence more than 2,000 m from the train, especially if the stations are spaced far apart. This statement becomes evident when standing on a platform feeling the airflow of an approaching train, especially in cases when the train is traversing a lengthy tunnel section, such as an under-river crossing (e.g., Manhattan-bound 7-Line trains at Grand Central Station in New York City or downtown San Francisco-bound trains at Embarcadero Station).

2.1.1.2 Boundary Conditions

At the junction between segments, mass continuity is enforced such that the mass of fluid entering a junction must equal the mass exiting:

$$\sum_{i=1}^{N_{in}} \rho\, U_i\, A_i = \sum_{j=1}^{N_{out}} \rho\, U_j\, A_j,$$

where $\rho\, U_i A_i$ is the mass flow into the junction from segment i, N_{in} is the number of inflows at the junction, $\rho\, U_j A_j$ is the mass flow away from the junction, and N_{out} is the number of outflows at the junction.

The static pressure at junctions is assumed to be equal. The static pressure at all vents, station entrances, and portals is assumed to equal atmospheric pressure.[2] This assumption is sometimes not fully correct as local pressure differences are known to cause inflows and outflows at stations or vents owing to building pressure effects, for instance on the leeward and windward sides of buildings, or due to stack effects. These effects, if known *a priori,* can be accounted for by specifying the flow velocity in vents, station entrances, or portals as described further in Section 2.2.

2.1.1.3 Method of Solution

The solution of the mechanical energy equation for the airflow in the subway tunnels and into/out of the vents, station entrances, and portals closely follows the SES approach. Sections 3.1 and 3.2 of the *Subway Environmental Design Handbook* (DOT 1976) provide a detailed description of the solution methodology, along with examples worked through by the authors; consequently, only an overview of the method is presented here.

[2] This state of equal atmospheric pressure is generally not the case and in fact is one of the key sources of naturally occurring airflows in the subway. Specifications of these pressures are very difficult, however, and require a building-aware atmospheric flow model such as Los Alamos National Laboratory QUIC modeling suite. See http://www.lanl.gov/projects/quic/quicpressure.shtml.

The solution methodology comprises four main steps:

1. Sum the loss coefficients and calculate the flow splits at each connection to the tunnel (e.g., vents, station entrances, or other tunnels).

2. Calculate the volumetric airflow rate caused by a train.

3. Use the flow splits and train-induced airflow rate to calculate the contribution to the flow rates in the subway tunnel and connections.

4. Repeat steps 1–3 to calculate and sum the contributions from all trains.

To calculate the flow split at the vent connection depicted in Figure 3, write the mechanical energy equation for the tunnel at location 2 and for the vent as

$$\frac{P_2 - P_\infty}{\rho/2} = K_2 U_2^2;$$
$$\frac{P_0 - P_\infty}{\rho/2} = K_v U_v^2.$$

P_0 is the stagnation pressure at the bottom of the vent shaft, assumed equal to P_2; P_∞ is atmospheric pressure; and K_v is the vent shaft loss coefficient. K_2 is the loss coefficient for the tunnel outward from location 2, which is the sum of the friction and form losses from location 2 to the aboveground portal.

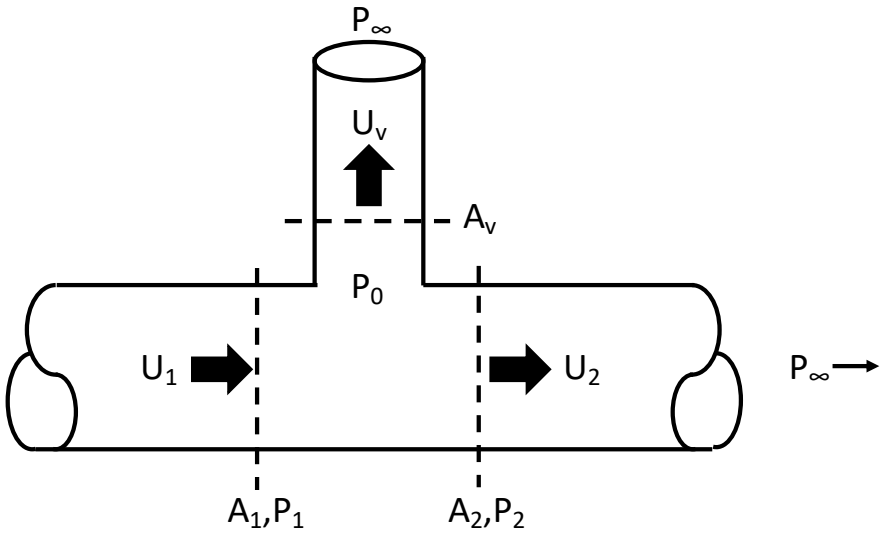

Figure 3. Schematic of outflow at a vent connection.

Combining the mechanical energy equations yields

$$K_2 U_2^2 = K_v U_v^2 \rightarrow \frac{U_2}{U_v} = \left(\frac{K_v}{K_2}\right)^{1/2}.$$

The flow split, that is, the ratio of the flow through the vent shaft to the flow through the tunnel at location 1, is

$$f_v = \frac{A_v U_v}{A_1 U_1} = \frac{A_v U_v}{A_2 U_2 + A_v U_v} = \left[1 + \frac{A_2 U_2}{A_v U_v}\right]^{-1} = \left[1 + \frac{A_2}{A_v}\left(\frac{K_v}{K_2}\right)^{\frac{1}{2}}\right]^{-1}$$
$$= \frac{1 - \sqrt{\alpha}}{1 - \alpha}; \alpha = \frac{K_v}{K_2}\left(\frac{A_2}{A_v}\right)^2.$$

The equivalent loss coefficient at location 1, which combines the losses in the vent shaft and the tunnel outward from location 2, is determined in a similar way:

$$f_v = \frac{A_v U_v}{A_1 U_1} = \frac{A_v}{A_1}\left(\frac{K_1}{K_v}\right)^{\frac{1}{2}} \rightarrow K_1 = K_v\left(\frac{A_1}{A_v}\right)^2 f_v^2 = K_2\left(\frac{A_1}{A_2}\right)^2 (1 - f_v)^2.$$

The calculation begins at the first connection inward from the portal such that K_2 is the sum of the friction loss from location 2 to the portal and the form loss arising from the rapid expansion at the portal: $K = [1 - (A_{inside}/A_{outside})]^2 = 1$ (Crane Valve Co. 1981). The calculation then proceeds inward until reaching the front of the train where K_f equals the equivalent loss coefficient from the connection nearest the train to the portal plus the friction loss between the train and vent.

A similar procedure is used to sum the loss coefficients and find the flow splits behind the train to find K_b. In these calculations, we also consider crossing subway tunnels by determining equivalent K's for both sides of the connection (i.e., for the tunnels on either side of the connection). Here, we step through the procedure outlined above from the portal or a set distance of the intersecting line to that connection to determine an effective *K*, which then serves to determine the flows to and from that connection. In this overall approach, we consider only the crossing tunnel closest to the train on both the front and back. Because most subways only have one or two crossline connections on any given line, limiting consideration to the one closest to the train is sufficient and computationally manageable. One obvious exception is the New York City subway, which is highly interconnected and therefore more challenging to model; however, through careful attention to the intersecting train lines and station layouts, realistic flow and dispersion results can be achieved even in complex stations such as Times Square.

The piston flow is calculated from the drag coefficient for the train:

$$C_D = \frac{\left(P_f - P_b\right) A_{train}}{\left(\frac{\rho U^2}{2}\right) A_{tunnel}} = \frac{\beta^2}{\sigma}\left(K_f + K_b\right),$$

where P_f and P_b and K_f and K_b are, respectively, the pressures and loss coefficients in front and back of the train; $\beta = U/V$, the ratio of the airflow velocity U to the actual train velocity V; and $\sigma = A_{train}/A_{tunnel}$ is the ratio of the cross-sectional area of the train to that of the tunnel. An empirical relationship for the drag coefficient is given in the DOT (1976) handbook[3] as follows:

$$C_D = C_{D\infty}(1-\beta)^2;$$
$$C_{D\infty} = 1.5\left(\frac{l/d}{15}\right)^{0.55} exp(0.68 + 1.13\sigma + 6.01\sigma^2),$$

where l and d are, respectively, the length and hydraulic diameter of the train. The expressions for the drag coefficient may be combined and solved for β:

$$\beta = \frac{1-\sqrt{\alpha}}{1-\alpha};$$
$$\alpha = \frac{\left(K_f + K_b\right)}{\sigma\, C_{D\infty}}.$$

Then, the airflow velocity arising from the piston flow is

$$U = \beta\, \gamma\, V,$$

where $\gamma = 1.2\sqrt{\sigma}$ (DOT 1976[4]) accounts for the reduction in the piston flow as the tunnel cross-sectional area increases, that is, the piston flow will be lower in a four-track tunnel than in a two-track tunnel. The volumetric flow rate induced by this train is $Q = UA_{tunnel}$, where

$$A_{tunnel} = \frac{1}{2}\left\{\left[\left(1+f_{open}\right)A_{seg}\right]_{front} + \left[\left(1+f_{open}\right)A_{seg}\right]_{back}\right\};$$

A_{seg} is the cross-sectional area of the tunnel segment in the direction of the train travel, and f_{open} is the fraction that the segment is open to the opposing direction of travel; for example, for a solid partition wall, $f_{open} = 0$, and for no partition between tracks, $f_{open} = 1$. The flow splits are then applied to calculate the contribution of this train to the flow rate in this tunnel; in the closest connecting tunnel, if any; and through the vents, station entrances, and portals. The process is repeated for all trains to determine the total flow throughout the subway system.

2.1.2 Subway Architecture Description

A typical subway configuration involves one or more lines of paired tunnels enabling bidirectional train operation, which may have partitions between them (solid or with periodic gaps) for fire safety purposes but may be completely open to each other at crossover locations and stations. Tunnel designs reflect the variety of construction challenges engineers and builders

[3] Equation 3.46 and Figure 3.31.

[4] Figure B.39.

have encountered and the solutions they developed; these include rectangular "cut-and-cover" tunnels located beneath city streets, semicircular "horseshoe" tunnels for deeper portions, circular tunnels bored through rock or under bodies of water, or circular cast iron "tubes" for underwater passages. Station designs range from merely a widening of the tunnel in older systems to airy, vaulted spaces in newer systems.

As described earlier, the complex network of tunnels, ventilation shafts, stations, station exits, and their interconnections that comprise a subway system is represented in BGM as a series of segments having specified attributes. For tunnel and station segments, these attributes include (1) the track coordinate location of the beginning of the segment (the end of a segment is defined by the beginning of the subsequent segment); (2) the cross-sectional area; (3) the shape, whether circular or rectangular, of the cross-section; (4) the fraction open to the opposing direction tunnel; and (5) the Darcy-Weisbach friction factor for the segment. For vents and station exits (i.e., connections to the outdoor environment), attributes include (1) the track coordinate of the connection; (2) the cross-sectional area; (3) the volume; and (4) the loss coefficients for outflow from the subway and for inflow from the outdoors.

Most of these attributes may be derived from design drawings and specifications. Determination of the friction factors and loss coefficients are described below.

2.1.2.1 Friction Factors in Subway Tunnels

Most handbooks limit the discussion of friction factors to pipes with uniform wall roughness, graphically depicted by the well-known Moody diagram in terms of relative roughness *r,* which is the ratio of the average height of the surface roughness elements *k* to the pipe diameter *D,* and the Reynolds number, Re = DU/ν, where ν is the kinematic viscosity. This treatment may be summarized for the limits of *smooth* and *rough* pipes (Schlichting 1979) as:

$$\frac{1}{\sqrt{f}} = 2\log_{10}\left(Re\sqrt{f}\right) - 0.8; \quad Re\sqrt{f/8}\,\frac{k}{D} \le 5 \;\; (smooth); \text{and}$$

$$\frac{1}{\sqrt{f}} = 2\log_{10}\frac{D}{k} + 1.14; \qquad Re\sqrt{f/8}\,\frac{k}{D} \ge 70 \;\; (rough).$$

For a typical subway tunnel, D_H = 5 m; with $\nu = 1.5\times10^{-5}$ m^2/s for air and an airflow velocity U = 10 m/s (22 miles hr^{-1}), Re = 3.3×10^6. In addition, for a typical subway tunnel, $k/D \sim 0.001$ so that f = 0.02 and $Re\sqrt{f/8}\,\frac{k}{D}$ = 166, which is well into the rough regime, where the friction factor is independent of *Re* and, therefore, independent of the airflow velocity. Accordingly, in BGM the friction factor is considered a static property that does not vary with airflow velocity.

Friction factors in subway tunnels and stations include contributions from a variety of elements in addition to the walls. The DOT (1976) handbook provides a helpful introduction to friction factors and presents an example for a circular, one-track tunnel in the Bay Area Rapid Transit

(BART) subway.[5] Appendix A presents our determination of friction factors for cut-and-cover tunnels, horseshoe tunnels, and cast iron tubes in the New York City subway, which more thoroughly illustrates the range of possible friction factors.

2.1.2.2 Loss Coefficients in Subways

The *SES Handbook* (DOT 1976[6]) provides a helpful introduction to loss coefficients, along with example calculations for a typical vent shaft. Additional helpful references include ASHRAE (2001) and Crane Valve Co. (1981).

As noted earlier, the value of K for a segment representing a vent or station exit is usually the *effective* loss coefficient, which results from combining all of the loss coefficients for that vent or station exit. When the contributors to the resistance occur in a series (e.g., a series of 90° turns in a vent shaft or stairway), the loss coefficients are additive but must be referenced to the same cross-sectional area, normally the smallest. Consider two loss coefficients K_1 and K_2 acting over areas A_1 and A_2. Mass conservation requires the flow through both portions to be equal, $U_1 A_1 = U_2 A_2$ or $U_2 = U_1(A_1/A_2)$. Summing the losses,

$$K_1 U_1^2 + K_2 U_2^2 = U_1^2 \left(K_1 + K_2 \left(\frac{A_1}{A_2} \right)^2 \right),$$

or

$$K_{eff} = K_1 + K_2 \left(\frac{A_1}{A_2} \right)^2,$$

where K_{eff} is referenced to area A_1.

For reasons of computational efficiency, it is often useful to combine the losses of multiple, parallel exits into a single effective exit. In this case, the reciprocals of the loss coefficients are summed. For N parallel losses and K_i acting over different areas A_i, the effective loss coefficient K_{eff} referenced to the sum of the areas A is

$$\frac{1}{K_{eff}} = \frac{1}{A^2} \left[\sum_{i=1}^{N} \frac{A_i}{\sqrt{K_i}} \right]^2 ; A = \sum_{i-1}^{N} A_i.$$

2.1.3 Train Movements

In addition to a description of the system architecture, the BGM airflow model requires the specification of the time-dependent position, velocity, and door condition (open/closed) of the subway trains. BGM can utilize actual data supplied by a subway system — when comparing model predictions with tracer study data for validation purposes or for real-time emergency

[5] See pages 3-25–3-29.

[6] See pages 3-29–3-34.

response — or the train data may be calculated based on the published schedules (e.g., weekday, weekend, nighttime) and train parameters, such as acceleration and deceleration rates and typical station dwell times. The calculation is performed external to BGM because the train data only need to be determined once for typical applications. However, modifications to the train operations (e.g., skipping a station, stopping all trains) in reaction to patron responses to a chemical release are handled internal to BGM.

The BGM train calculations are similar to those carried out by SES with the exception that the heat generation calculations are not included because BGM does not calculate the subway temperature distribution. In addition, the BGM train model accounts for the possibility that the same train may make multiple trips along the same route. For example, when a contaminated southbound train reaches the end of the line, if a northbound departure is scheduled within a specified time, the following occurs: the airborne material concentration, the mass deposited on train car surfaces, and the mass accumulated in train car filters are transferred to the cars of the northbound train. If no northbound departure is scheduled within the specified time, it is assumed that the southbound train goes out of service (i.e., moves to a marshaling yard).

2.2 Airflow by Natural Ventilation

Although the motion of the trains is the primary driver of airflows in the subway, it is not the only driver. Temperature differences within the subway and between the subway and the aboveground environment can give rise to airflows caused by thermal buoyancy differences (so-called “stack flows”). In addition, wind-driven dynamic pressure forces at portals, vent openings, and station exits can also induce airflows in the subway, depending on wind speed and direction relative to the subway openings.

Figure 4 presents measurements of airflow velocity and temperature in the Washington, D.C., subway that reveal the presence of natural flows: after revenue service ends at about 2:00 a.m., cooler air is drawn into the subway as warmer air rises and flows out, causing the temperature in the subway to drop. As the temperature drops, the indoor-outdoor temperature difference decreases, which reduces the stack flow and the indoor temperature rises again after 3:00 a.m. until the temperature difference increases sufficiently for the stack flow to re-assert itself.

BGM does not explicitly calculate airflows arising from thermal buoyancy or wind pressure; however, BGM does have the capability to incorporate prescribed “background” airflow caused by non-train effects or forced ventilation. This treatment is accomplished by imposing fixed flows at station entrances, vent shafts, or portals, as well as prescribing airflows between subway lines at crossover stations.

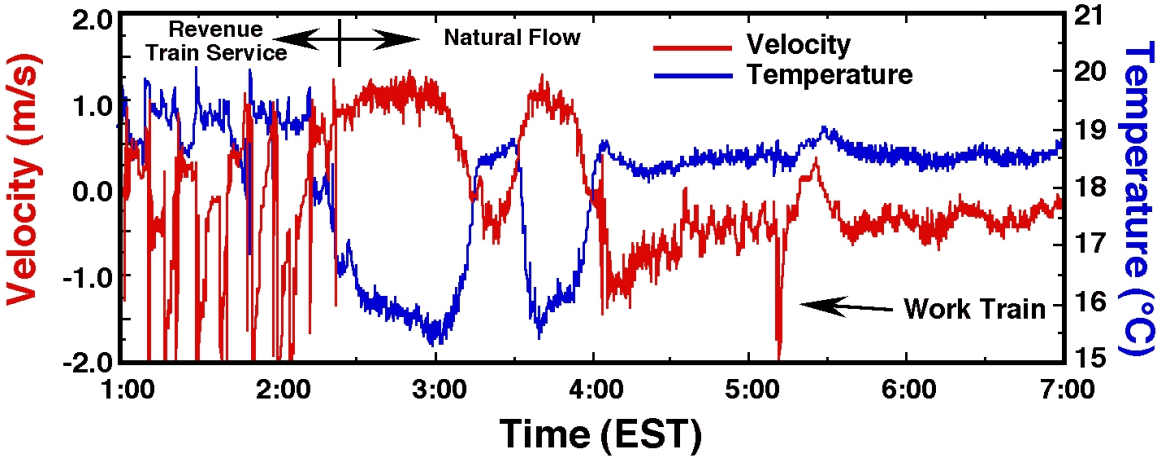

Figure 4. Measured airflow velocity and temperature in the Washington, D.C., subway.

Because the magnitude of these natural airflows depends on meteorological conditions and, to some degree, on train operations, their effect is to add variability to the train-forced airflows. The degree of variability depends on the subway configuration: subways with more aboveground connections experience a greater influence by natural ventilation effects than subways with fewer connections. In addition, the influence of these flows increases as the train frequency and/or speeds decrease.

3 Transport and Dispersion in the Subway

3.1 Theoretical Basis

The one-dimensional transport and dispersion of mean material concentration C(x,t) in a turbulent flow of an incompressible fluid is described by Hinze (1975[7]) as:

$$\frac{\partial C}{\partial t} + U\frac{\partial C}{\partial x} = -\frac{\partial}{\partial x}\overline{u'c'} + S,$$

where the concentration and fluid velocity are expressed in terms of their respective mean values C, U, and turbulent fluctuations c' and u'; where x is position, and t is time. S is a source or sink term, which may represent the initial release of material, the uptake and emission of material by the train cars, deposition onto subway surfaces, or the deposition and subsequent resuspension of material from subway patrons.

The term $U\,\partial C/\partial x$ represents the advection of material by the mean flow velocity, which was calculated using the airflow model. The term $\overline{u'c'}$ represents the diffusion of material by fluid turbulence. By analogy to molecular diffusion (which is negligible in comparison), turbulent diffusion is assumed to be proportional to the mean concentration gradient by K, the "coefficient of eddy diffusion" (Hinze 1975[8]), as given in:

$$\overline{u'c'} = -K\frac{\partial C}{\partial x}.$$

Substituting this expression yields the one-dimensional advection-diffusion equation:

$$\frac{\partial C}{\partial t} + U\frac{\partial C}{\partial x} = K\frac{\partial^2 C}{\partial x^2} + S.$$

The eddy diffusion coefficient for the dispersion of material in turbulent flow in a pipe is proportional to the mean flow velocity (Taylor 1954)

$$K = 5.05\,D\,U\left(\frac{u_*}{U}\right) = 5.05\,D\,U\sqrt{\frac{f}{8}} = 1.785\,D\,U\sqrt{f}\,,$$

where D is the pipe diameter (or hydraulic diameter for a non-circular duct), U is the mean flow velocity, u_* is the friction velocity, and f is the familiar Darcy-Weisbach friction factor.

In their implementation of the advection-diffusion equation, Winkler et al. (2006) used an expression for f as a function of the Reynolds number, which is valid for smooth pipes and Re <

[7] See page 378, Equation 5-34.

[8] See page 379.

10^5. For a typical subway tunnel D_H = 5 m, ν = 1.5×10^{-5} m^2/s, so that Re = 10^5 corresponds to U = 0.3 m/s (< 1 mile per hour). For the large Reynolds numbers and aerodynamic roughness conditions encountered in the subway, the friction factor is independent of Re as demonstrated earlier.

In our application, we further simplify this expression by assuming that $u_*/U = 1/7$. This treatment reduces the above expression to

$$K = \alpha\, D\, U,$$

where α = 0.72. Through testing this expression in realistic subway cases, it is apparent that results are roughly the same for values of α ranging from 0.2 to 0.72. Therefore for most applications, we set α to 0.3 to speed execution as often the diffusion term is the limiting factor in ensuring computational stability, as discussed in the following section.

3.1.1 Method of Solution

The advection-diffusion equation is solved numerically using the method of MacCormack (Anderson, Tannehill, and Pletcher 1984[9]), which is second-order accurate in both time and space. At the beginning of the simulation, the segments describing the subway system are subdivided into computational grid cells according to the user-specified spatial resolution Δx. The time step Δt is then selected to satisfy the Courant-Fredrichs-Levy (CFL) condition (Anderson, Tannehill, and Pletcher 1984[10]) to ensure that information does not propagate more than one computational cell in a single time step, thus avoiding an instability known as "numerical diffusion." For the MacCormack method, the CFL condition (Anderson, Tannehill, and Pletcher 1984) is

$$\frac{U\Delta t}{\Delta x} + \frac{2K\Delta t}{(\Delta x)^2} \leq 1.$$

Substituting the expression for the eddy diffusion coefficient, this treatment becomes

$$\frac{U\Delta t}{\Delta x}\left(1 + \frac{2\,\alpha\,D_H}{\Delta x}\right) \leq 1.$$

To ensure stability in BGM calculations, the condition outlined above is modified to be ≤ 0.75. For a given spatial resolution, this condition requires a smaller time step (and therefore increased computational time) for segments with high airflow velocities. As noted earlier, a value of α = 0.3 is generally used, which is reasonable for most subway tunnels and stations.

[9] See page 163.

[10] See page 75.

3.1.2 Boundary Conditions

In a similar fashion to the airflow calculations, conservation of contaminant mass is enforced at the segment junctions as

$$\sum_{i=1}^{N_{in}} C_i\, U_i\, A_i = \sum_{j=1}^{N_{out}} C_j\, U_j\, A_j\,,$$

where $C_i U_i A_i$ is the contaminant mass flow into the junction from segment i, N_{in} is the number of inflows at the junction, $C_j U_j A_j$ is the contaminant mass flow away from the junction, and N_{out} is the number of outflows at the junction. In addition, the fraction of contaminant mass in each outflow segment relative to the sum of the contaminant outflows is identical to the fraction of airflow in each outflow segment relative to the total outflowing air, that is,

$$\frac{C_j U_j A_j}{\sum_{j=1}^{N_{out}} C_j\, U_j\, A_j} = \frac{U_j A_j}{\sum_{j=1}^{N_{out}} U_j\, A_j}\,.$$

At all connections with the outdoor environment, the airborne concentration is set to zero. The contaminant mass exiting at these connections is subtracted from the airborne mass in the simulation. However, the time-varying contaminant mass fluxes at each of these locations are retained (at a user-specified averaging period) for subsequent analysis, for example, as sources to aboveground dispersion models.

For the reasons above, we consider concentration, dosage, and deposition predictions of the Argonne BGM model to be order-of-magnitude type estimates. This approach is generally sufficient to inform detector specification and siting studies and to guide mitigation strategies. However, in evaluating the results of any particular model run or analysis, these uncertainties should be kept in mind.

3.2 Train Car Exchange

As discussed in Section 1.2, train cars are a critical component of the subway transport dispersion problem. While the trains create airflow in the system that acts to spread and disperse the contaminant, the individual train cars take in and release the contaminant, thus becoming moving sources that transport the contaminant at the speed of the trains. Both modeling and experimental observations have shown that the first arrival of contaminants at remote locations from the source is governed by the speed of the trains rather than airflow considerations. Train cars can take in relatively large amounts of airborne material at scheduled stops and then release this material continuously as they travel.

The velocity and position of trains within BGM are calculated according to pre-specified train schedules, which are either estimated based on published schedules or determined using real-time train position and velocity data provided in an operational data stream. Trains have a given

number of cars ranging from 2 to 11 depending on the system and subway line. In turn, each train car within BGM is treated as a single-zone building with an HVAC system that has both fresh air and recirculation air streams. In this framework, we define several parameters, as illustrated in Figure 5. These include fresh air intake rate, recirculation rate, filter efficiency, and train car volume.

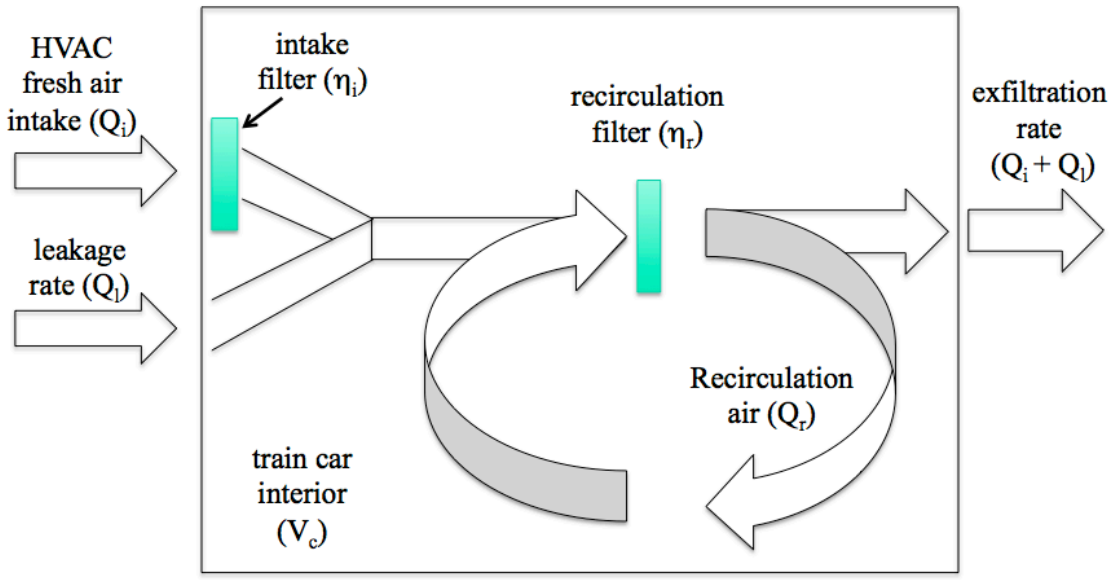

Figure 5. Diagram illustrating the parameters used in the single-zone HVAC model for each train car.

Removal of particulate material from fresh and recirculation air streams by the train car filters is accounted for in the train car calculations through the filtration efficiency. Figure 6 shows the filtration efficiencies used; individual train car filter efficiencies are chosen randomly from the distribution shown in the box and whisker plots. For context, select test data for subway filter efficiency are also shown. The BGM filter efficiencies are available for the particle size range from 0.1 to 50 microns.

Particulate removal by the station HVAC systems is also accounted for in BGM, although few subways in the United States have them. The systems that do have station HVAC are in Washington, D.C. (summer only), Los Angeles, Seattle, and the newest stations in New York City. The station filtration system in the Washington, D.C., subway is less effective than train car filtration because relatively inefficient roll filters (at approximately a minimum efficiency reporting value [MERV] of 4) have historically been used in the stations. The efficiency of these filters increases with use as debris loading increases; there are also particle losses in the HVAC ducts.

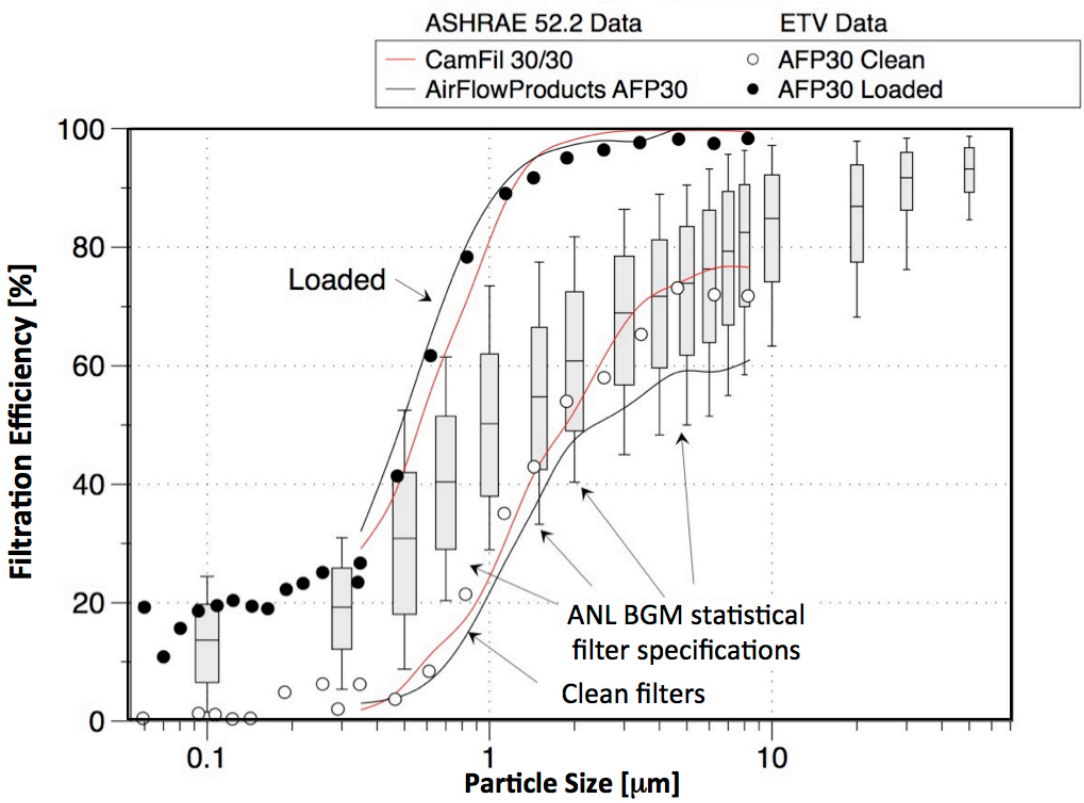

Figure 6. Filtration efficiencies used in the Argonne BGM train car model. The whiskers on the bars represent the 10th and 90th percentiles, the box edges represent 25th and 75th percentiles, and the centerline indicates the median (50th percentile) value. Filter efficiency measurements for select filters are provided for context. Figure courtesy of Dr. Woody Delp (Lawrence Berkeley National Laboratory).

3.3 Source Models

There are a variety of different source models and types that can be treated within BGM. These include:

- A fixed-point source
- A moving source (on train)
- Constant release rate, finite duration
- Evaporative (variable release rate, duration based on amount released)

There is no limit to the number of sources that can be considered in a single model run. In addition to the source emission amounts, a monodisperse particle size for biological or radiological agents is also specified. All sources in an individual model run must have the same particle size.

This page intentionally left blank.

4 Deposition of Particulate Materials

The rate of deposition of particle mass *m* onto tunnel, station, or train car surfaces at a given time and location is modeled as

$$\frac{dm}{dt} = V_d C\, A_s\,,$$

where V_d is the deposition velocity, C is the airborne mass concentration, and A_s is the surface area of the tunnel or station segment or train car. For the airborne concentration, mass conservation requires

$$\frac{dC}{dt} = -V_d C\, \frac{A_s}{\tilde{V}}\,,$$

where $\tilde{V}$ is the volume of the tunnel or station segment or train car. A positive deposition velocity indicates particle movement from the air toward the surface.

The deposition velocity for the floor, walls, and ceiling are calculated by combining, as appropriate, contributions from settling V_g, forced or natural convection V_c, and thermophoresis V_t:

$$V_{floor} = V_g + V_c + V_t\,;$$
$$V_{wall} = V_c + V_t\,;$$
$$V_{ceiling} = -V_g + V_c + V_t\,.$$

The overall deposition velocity is calculated by combining these contributions:

$$V_d = \tfrac{1}{4}\left(V_{floor} + 2\,\mathrm{V}_{wall} + V_{ceiling}\right).$$

Detailed descriptions of the algorithms for calculating deposition velocities from settling, forced and natural convection, and thermophoresis are presented in Appendix B.

Whether forced and/or natural convection contributions are used to determine V_c depends on the comparison between Grashoff and Reynolds numbers (Gr = Ra/Pr; refer to Appendix B for definitions). If $\mathrm{Gr} < \mathrm{Re}^2$, forced convection is the dominant transport mechanism, whereas if $\mathrm{Gr} > 10\ \mathrm{Re}^2$, natural convection is the dominant transport mechanism. In the intermediate range, deposition velocities for both forced and natural convection are determined, and the larger value is chosen.

This page intentionally left blank.

5 Adsorption and Desorption of Gaseous Agents

To account for gas adsorption and desorption with subway surfaces, BGM uses a "2-sink" model (Singer et al. 2005, 2007) wherein airborne material is adsorbed by, or desorbed from, a surface layer, which, in turn, exchanges material by diffusion with a substrate layer that is not exposed to the air. These exchanges are described by the following set of equations:

$$\frac{dC}{dt} = -\lambda_a C + \lambda_d \frac{m_1}{\tilde{V}};$$
$$\frac{dm_1}{dt} = -(\lambda_d + k_1)m_1 + \lambda_a C\tilde{V} + k_2 m_2;$$
$$\frac{dm_2}{dt} = -k_2 m_2 + k_1 m_1.$$

Here, C is the airborne mass concentration; m_1 and m_2 are the masses contained in the surface and substrate layers, respectively; $\tilde{V}$ is the volume of the train car or tunnel/station segment; and λ_a, λ_d, k_1, and k_2 are the rate constants for adsorption by the surface, desorption from the surface, diffusion from the surface to the substrate, and diffusion from the substrate to the surface, respectively. The determination of the rate constants is discussed in Appendix C.

The effect of sorption is to reduce the airborne concentration initially, as material is adsorbed by surfaces, but then to reduce the rate at which the concentration declines as material desorbs from surfaces. This sorption pattern can have an ameliorative effect on health consequences at least initially by reducing the peak concentration, depending on the subway surface materials and their rate constants.

This page intentionally left blank.

6 Model Validation

6.1 Validation of the Airflow Model

Beginning in November 2001 and continuing through November 2005, 10 airflow monitoring systems were deployed in the Washington, D.C., subway to measure airflow speed, direction, temperature, and pressure to characterize natural flows in the tunnels, as shown in Figure 4. Operational subway data were also recorded, including train position and speed, as well as fan and vent shaft louver settings. Meteorological data were obtained from monitoring stations at Reagan National Airport and other locations in the downtown area. Additional airflow measurements were carried out at 22 stations to characterize the airflow into and out of the subway. Figure 7 presents a comparison of measured and modeled airflows at the Metro Center Station, demonstrating the high fidelity of the airflow model.

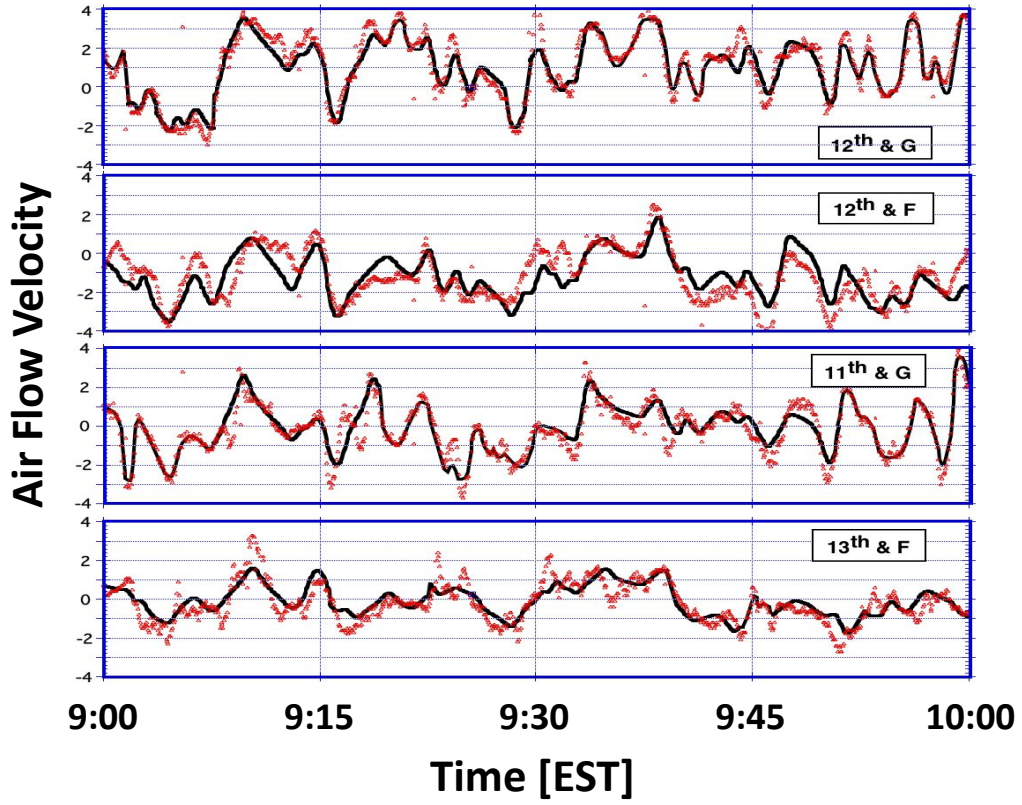

Figure 7. Measured (symbols) and modeled (solid line) airflow velocity at four entrances to the Metro Center Station in the Washington, D.C., subway. Positive values indicate airflow out of the subway station.

6.2 Validation of the Transport and Dispersion Model

As discussed in Section 1.1, measurement campaigns have been conducted in several major subway systems for model validation purposes. In these studies, gas and particulate tracers were released in the subway accompanied by simultaneous measurements throughout the system, as follows:

- Time-varying concentrations on many station platforms;
- Time-varying concentrations in train cars; and
- Material fluxes at selected vents and station entrances.

Figure 8 presents a comparison of measured and modeled time-integrated airborne concentrations (dosages) for the gas tracers released in the Washington, D.C., subway during the 2007 and 2008 test periods (Brown et al. 2009). The model simulations utilized operational information supplied by the subway, including train position and speed, as well as fan and vent shaft louver settings.

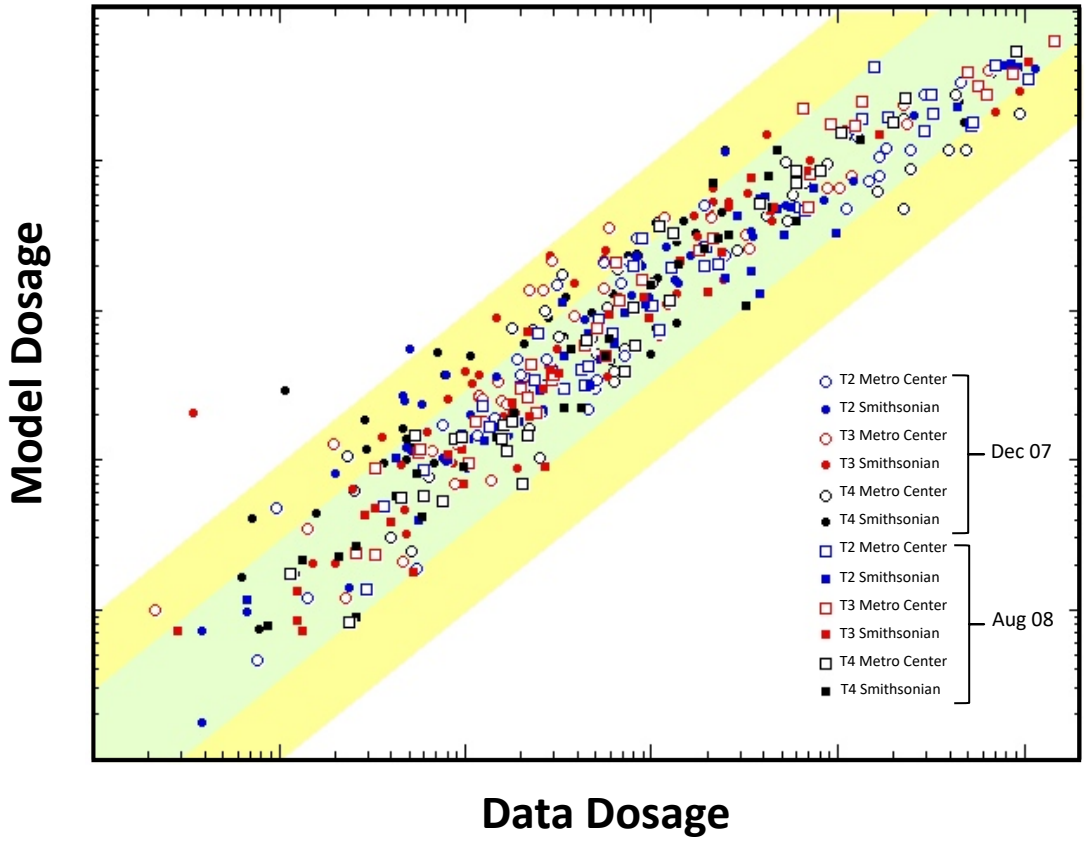

Figure 8. Measured and modeled dosages for gas tracers released in the Washington, D.C., subway. The logarithmic scales span five orders of magnitude. (Numerical labels have been deliberately omitted.) The green and yellow bands indicate factors of ±3 and ±10, respectively.

The comparison demonstrates that 68% of the model predictions are within a factor of 3, and 95% are within a factor of 10. The comparison also reveals that at the highest dosages — near the tracer release locations — the model under-predicts slightly. This result is a consequence of the one-dimensional representation of the subway. In reality, material released at a point will take time to disperse transverse with respect to the direction of the airflow such that measurements near the source will record higher concentrations initially than the cross-sectional average predicted by the model.

The Washington, D.C., subway has a limited number of vents, primarily "blast shafts" located at the ends of station platforms to mitigate the rapid rise in pressure and airflow caused by an approaching train. In contrast, the New York City subway has many street-level vents along the stations and tunnels, which result in a greater influence of the aboveground meteorology and more variability in the natural airflows in the subway. A comparison of model-predicted dosages with measured gas tracer data obtained in the New York City subway (Ervin et al. 2018) presented in Figure 9 exhibits more variability than for similar results in the Washington, D.C., subway. Although the model predictions utilized the nominal train schedule rather than actual train position and speed data, the increased variability is more likely a result of natural airflows and the highly interconnected nature of the system.

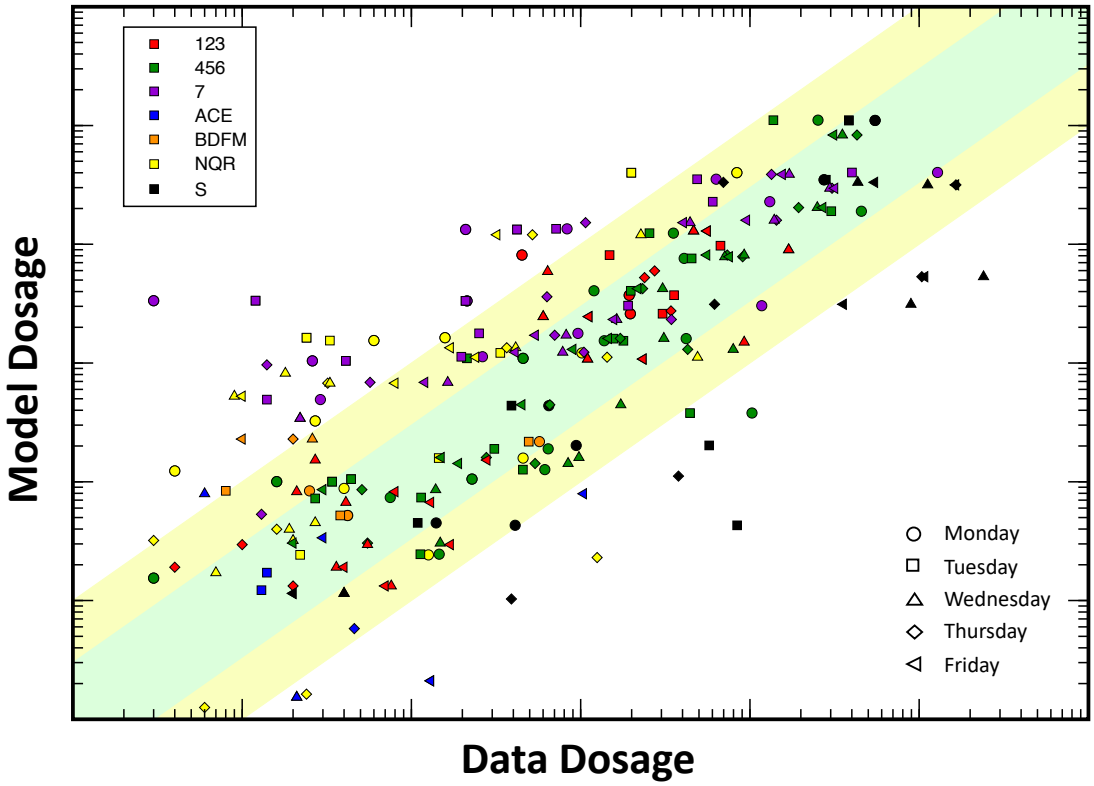

Figure 9. Measured and modeled dosages for gas tracers released in the New York City subway. Colors indicate the subway line where the measurements were acquired; symbols indicate the day of the test.

In Figure 10, the residuals of the comparison in Figure 9 are presented in a log-probability format, along with a straight line representing a log-normal distribution having the same median and geometric standard deviation (GSD) as the residuals. The evident log-normal distribution of the residuals suggests that the model largely captures the phenomenology. The median is close to unity, which suggests the model is largely unbiased. The GSD indicates that 68% of the model predictions are within a factor of 6.4 of the data and 95% are within a factor of 40 — about twice the variability observed in the Washington, D.C., comparison.

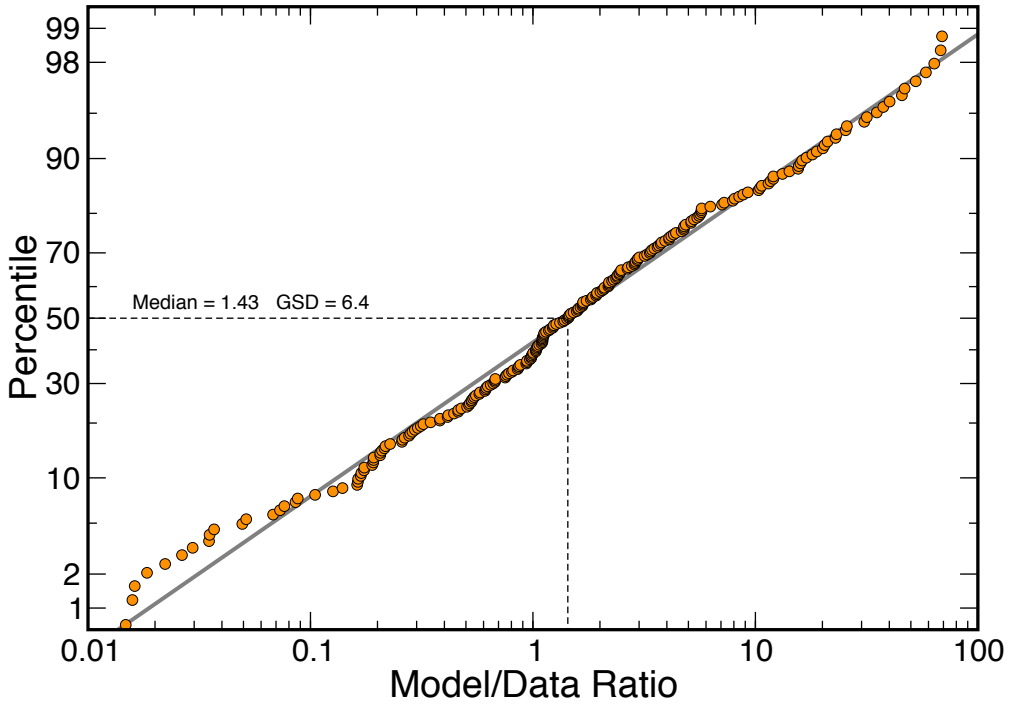

Figure 10. Residuals of the model-data comparison presented in Figure 9 (symbols) and a log-normal distribution (solid line) having the same median and geometric standard deviation.

Subsets of the comparison dataset for each subway line are presented in Figure 11. The Seventh Avenue Line (1/2/3 trains) and Lexington Avenue Line (4/5/6 trains) exhibit medians close to 1 and GSDs close to 3, in agreement with the Washington, D.C., results. Most of the tracer releases carried out in these tests occurred on these two subway lines, which have the largest ridership in the system. Although the natural flow in the Shuttle Line (S trains) connecting these two lines has been approximately accounted for in the simulations by assuming a 1-mile-per-hour flow either eastward or westward depending on the aboveground wind direction, the observed departure of the Shuttle Line residuals from the log-normal line likely results from inadequate estimation of the natural flow for some cases.

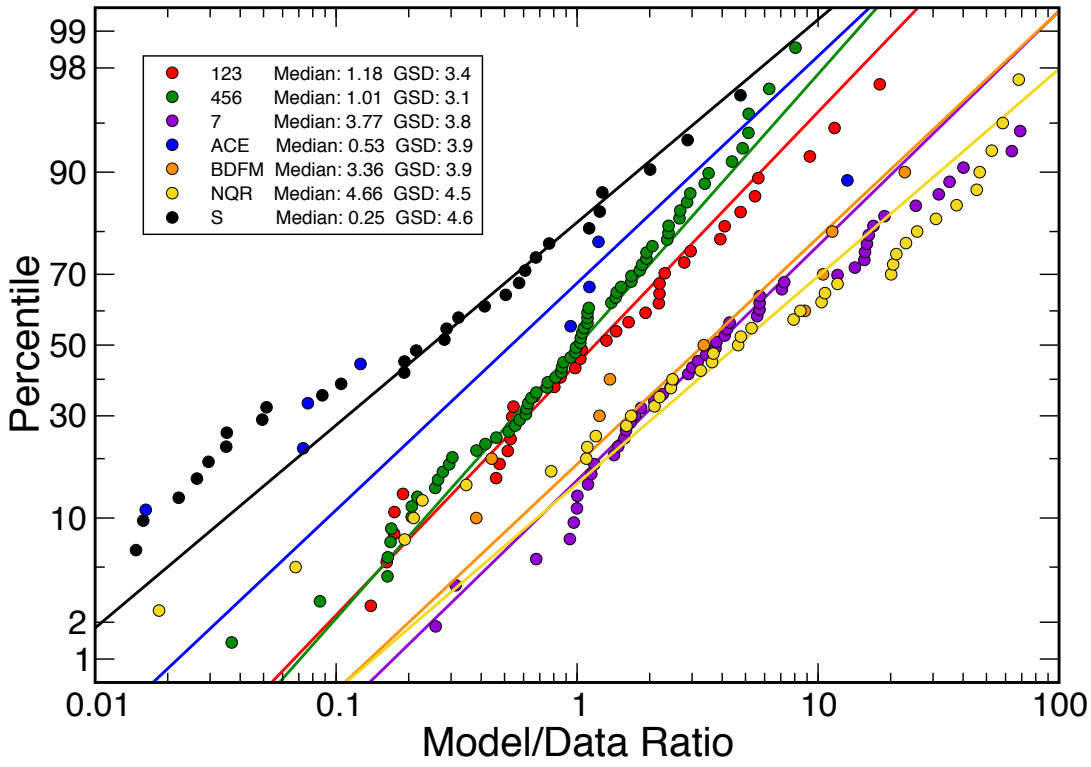

Figure 11. Residuals of the model-data comparison and log-normal distributions (solid lines) but displaying subsets for each subway line.

The GSDs of the other subway lines are only slightly larger, in the range 3.8–4.6, which suggests the modeled dispersion along those lines is largely correct; however, their medians vary by a factor of ±4, supporting the earlier assertion that the increased variability in the comparison arises from the highly interconnected nature of the system and the likely impact of natural airflows between lines to enhance or suppress the train-induced airflows. The increased variability in the full dataset highlights the challenges in predicting the material exchanges between subway lines, which can vary on a daily or even hourly basis depending on the aboveground meteorology. Nevertheless, the results demonstrate the high fidelity of the model even for a very complex subway system.

This page intentionally left blank.

7 Summary

The Argonne BGM was developed to provide a comprehensive simulation capability for analysis of subway threats at the level of the entire system. BGM predicts the movement and spread of a chemical or biological agent within an underground subway system, as well as the amount of material released to the environment through station entrances, street-level vents, and tunnel portals.

The BGM airflow model, based on the SES approach, has been validated against the results of extensive airflow measurements in the Washington, D.C., subway. Measurement campaigns in several subway systems involving the simultaneous release of multiple gas and particle tracers have been carried out to validate the material transport and dispersion model.

BGM has been used to conduct a wide range of analyses for many subways, such as determining the optimal chemical/biological detector architectures for subway systems, defining detector performance requirements, assessing the efficacy of response strategies, analyzing combined facility/outdoor/subway detector architecture, assessing chemical detector cost/performance, and predicting the potential impacts of fomite transport by rail transit passengers.

7.1 Limitations of the Model

The Argonne BGM provides useful insights concerning the magnitude and extent of chemical, biological, and radiological incidents originating in the subway (or outdoors and drawn into the subway) in conjunction with detection assets to mitigate consequences and aid a proper response. However, the model has significant uncertainties, the magnitude and importance of which include the following:

- The one-dimensional nature of the model does not permit a precise geometric representation of the stations, especially mezzanines and complex entrances. Furthermore, it cannot represent certain three-dimensional flow characteristics that frequently occur in open, multi-track tunnel systems or large stations. These effects on the bulk flow through the system are likely minimal but do have substantial implications when comparing concentration and dosage statistics at particular points within an individual subway station.

- Critical train car parameters, such as filter efficiency and leakage rates, are based on engineering specifications; however, actual train cars may exhibit considerable departures from these nominal values. In an effort to accommodate this variability, parameters such as train car or station filtration efficiency are modeled in a statistical fashion by specifying a distribution that is randomly sampled.

- Operation of forced ventilation systems in stations and tunnels, such as under platform exhaust and emergency ventilation fans, is based on engineering performance specifications provided by the transit systems. Ventilation system performance that

departs from these nominal values may significantly affect the results. In the absence of actual airflow test data, these values should be considered a best estimate.

- As discussed in Section 2.2, naturally occurring airflows in the subway that result from temperature differences or external weather can have a substantial influence on the transport and dispersion rates. These can be input to the model *a priori* but are not currently calculated by the model based on weather conditions or heat generated by trains and patrons. This capability may be added in later versions of BGM.

- Actual train schedules that depart significantly from the published schedules (generally weekday, Saturday, and Sunday) will potentially influence the results.

- Factors such as biological agent decay and deposition may vary considerably depending on local conditions. Their inclusion in the model is therefore approximate.

- Quantification of the effects of inhalation or deposition may be increasingly uncertain as the airborne concentration drops below 1 particle per liter given that the model is based on an average mass concentration with bulk removal processes based on particle size. This treatment can be an issue with larger particle sizes where inhalation of a single particle of a biological agent could have adverse health effects.

8 References

ASHRAE (American Society of Heating, Refrigeration, and Air-conditioning Engineers), 2001, Chapter 21, "Duct Design," in *Handbook of Fundamentals*.

Anderson, D.A., J.C. Tannehill, and R.H. Pletcher, 1984, *Computational Fluid Mechanics and Heat Transfer*, Hemisphere Publishing Co., New York.

Bejan, A., J.H. Boyett, and A.D. Kraus, 2003, *Heat Transfer Handbook*, Wiley-IEEE Publishing Corporation, New York.

Coke, L.R., J.G. Sanchez, and A.J. Policastro, 2000, "A Model for the Dispersion of Contaminants in the Subway Environment," in *Proc. 10th International Symposium on Aerodynamics and Ventilation of Vehicle Tunnels,* BHR Group, Boston, 279–303.

Crane Valve Co., 1981, Appendix A, pp. A-26–A-28, in *Flow of Fluids Through Valves, Fittings, and Pipes*, Technical Paper 410.

DOT (U.S. Department of Transportation), 1976, *Subway Environmental Design Handbook, Volume I: Principles and Applications*, *2nd Edition*, UMTA-DC-06-0010-76-1, John A. Volpe National Transportation Systems Center, Cambridge, Mass.

Ervin, B.L., Personal Communication, 20 November 2013.

Ervin, B.L., M. Virdi, C. Rudzinski, T. Vian, D.F. Brown, J.C. Liljegren, E.K. Wheeler, M. Frank, S. Kane, P. Kalb, T. Sullivan, J. Heiser, R. Wilke, and R. Maddalena, 2018, *Underground Transport Restoration (UTR): Particulate and Gas Dispersion Measurements in the NYC Subway and Surrounding Outdoor Environment,* Technical Report, Massachusetts Institute of Technology Lincoln Laboratory, Lexington, Mass.

Gebhart, B., Y. Jaluria, R.L. Mahajan, and B. Sammakia, 1988, *Buoyancy-Induced Flows and Transport*, Hemisphere Publishing Corporation, New York.

Hinze, J.O., 1975, *Turbulence*, 2nd Edition, McGraw-Hill, New York.

Hinds, W.C., 1982, *Aerosol Technology,* John Wiley & Sons, New York.

Kalb, P., 2014, unpublished report.

Kays, W.M., and M.E. Crawford, 1980, *Convective Heat and Mass Transfer*, 2nd Edition, McGraw-Hill, New York.

Karlsson, E., and U. Huber, 1996, "Influence of Desorption on the Indoor Concentration of Toxic Gases," *Journal of Hazardous Materials* 49, 15–27.

Liljegren, J.C., and D.F. Brown, 2014, *Argonne Below Ground Model Part II: Population Dynamics, Exposure, and Fomite Transport*, ANL/DIS-14/13, Argonne National Laboratory, Argonne, Ill.

McPherson, M.J., 1993, Subsurface Ventilation and Environmental Engineering, Chapman & Hall, London.

Nazaroff, W.W., and G.R. Cass, 1987, "Particle Deposition from a Natural Convection Flow onto a Vertical Isothermal Plate," *Journal of Aerosol Science* 15, 567–584.

Nazaroff, W.W., and G.R. Cass, 1989, "Mass-Transport Aspects of Pollutant Removal at Indoor Surfaces," *Environment International* 15, 567–584.

Schlichting, H., 1979, *Boundary-Layer Theory*, 7th Edition, McGraw-Hill, New York.

Shanes, I.H., 1962, *The Mechanics of Fluids*, McGraw-Hill, New York.

Singer, B.C., A.T. Hodgson, H. Destaillats, T. Hotchi, K.L. Rezvan, and R.G. Sextro, 2005, "Indoor Sorption of Surrogates for Sarin and Related Nerve Agents," *Environmental Science & Technology* 39, 3203–3214.

Singer, B.C., A.T. Hodgson, T. Hotchi, K.Y. Ming, R.G. Sextro, E.E. Wood, and N.J. Brown, 2007, Sorption of Organic Gases in Residential Rooms, *Atmospheric Environment* 41, 3251–3265.

Smithson, A., and L.-A. Levy, 2000, Chapter 3 in *Ataxia: The Chemical and Biological Terrorism Threat and the U.S. Response,* Report 35, Henry L. Stimson Center. Available at http://www.stimson.org/books-reports/ataxia-the-chemical-and-biological-terrorism-threat-and-the-us-response/ (accessed August 13, 2018).

Taylor, G.I., 1954, "The Dispersion of Matter in Turbulent Flow in a Pipe," *Proceedings of the Royal Society of London*, *Series A*, 223(1155), 446–468.

U.S. Army, 1966, "Test Tube Study: Results of Tests (U)," Special Operations Division, Fort Detrick, Maryland.

Winkler, S., G.R. Larocque, J.Z. Lin, E.T. Williamson, and T.J. Dasey, 2006, *Subway Biodefense Risk Model*, Technical Report ESC-TR-2006-064, Massachusetts Institute of Technology Lincoln Laboratory, Lexington, Mass.

Appendix A: Friction Factors in Subway Tunnels

Friction factors in subway tunnels and stations include contributions from a variety of elements in addition to the walls, which may be the least contributor. Here we present our determination of friction factors for cut-and-cover tunnels, horseshoe tunnels, and cast-iron tubes in the New York City subway, which illustrate the range of possible friction factors and the dominant contribution from free-standing support columns.

A.1 Cut-and-Cover Tunnels

The walls of cut-and-cover (c/c) tunnels are constructed from 12-in. I-beams, approximately 13 ft high and spaced every 5 ft on center along the axis of the tunnel. The wall columns are completely embedded in the concrete walls. The 15- to 18-in. I-beams are supported by the wall columns and, for multi-track tunnels, by rows of 6-in. steel columns spaced approximately every 13 ft on center across the width of the tunnel and oriented such that their flanges are parallel to the tunnel axis. Concrete arches between the roof beams form the tunnel roof. The tunnel floor is concrete.

The friction factor includes contributions from (1) the concrete walls and floor, (2) the roof beams, and (3) the support columns. These are summarized in Table A-1 and described in detail in the text that follows.

Table A-1. Friction Factors in C/C Tunnels

	1-track	2-track	3-track	4-track
Width × Height, ft	13 × 13	26 × 13	39 × 13	52 × 13
Column Spacing, λ	5	5	5	5
Hydraulic diameter, D_H, ft	14	20	24	27
λ/D_H	0.357	0.25	0.208	0.185
Relative roughness, k/D_H	0.0007	0.0005	0.00042	0.00037
$f_{wall/floor}$	0.018	0.017	0.0165	0.016
f_{roof}	0.37	0.23	0.17	0.14
$f_{columns}$	–	0.075	0.12	0.15
f_{tunnel}	0.11	0.16	0.19	0.22

The hydraulic diameter D_H was determined using the nomograph in Fig. 3.15 of the *SES Handbook* (DOT 1976). A wall roughness of $k = 0.01$ ft appropriate for "rough concrete" (Table 3.11, *SES Handbook*) was selected because of the age of tunnels. The wall friction factor f_{wall} was obtained from the Moody diagram in Fig. 3.14 of the *SES Handbook* based on the relative roughness k/D_H and assumes fully turbulent flow.

The contribution from the roof beams was determined by treating the beams as "ribs" and referring to Fig. 3.16 in the *SES Handbook*. We assumed 15-in. beams for one- and two-track tunnels, whereas 18-in. beams were assumed for three- and four-track tunnels.

For the columns, the friction factor was determined using the following expression from the mining literature (McPherson 1993[11]):

$$f = C_D \frac{A_{column}}{A_{tunnel}} \frac{D_H}{\lambda} F; \quad F = 0.0035\,\Delta + 0.44\,,$$

where C_D = 2.05 is the drag coefficient for an I-beam with the flanges parallel to the direction of airflow (McPherson 1993[12]), A_{column} is the area of the column normal to the airflow, and A_{tunnel} is the cross-sectional area of the tunnel. The wake interference of the columns is accounted for by the function F, which depends on the ratio of the column spacing to the column width, $\Delta = 5/0.5 = 10$.

The total friction factor is calculated by weighting the contributions of the walls/floor and roof according the fraction of the perimeter they affect and adding the column contribution. For a four-track tunnel, $f = 0.016\ (.60) + 0.14\ (.40) + 0.15 = 0.22$; for a two-track tunnel, $f = 0.017\ (.625) + 0.23\ (.375) + 0.075 = 0.16$.

For tunnels where the center row of columns has been replaced by a solid or porous wall, a friction factor corresponding to a tunnel with half the number of tracks is used; for example, for a four-track tunnel with a center wall, the friction factor for a two-track tunnel is used, whereas for a two-track tunnel, the friction factor for a one-track tunnel is used.

A.2 Horseshoe Tunnels

Horseshoe tunnels are so named because of the arched roof of reinforced concrete that replaces the exposed roof beam with support columns and transverse arches found in the c/c tunnels. Consequently, the horseshoe tunnels have a significantly lower friction factor than do the c/c tunnels. Accordingly, other relatively minor contributors to the friction factor, such as the track, power rail, etc., that are ignored for the c/c tunnels must be considered for the horseshoe tunnels. Estimates for the friction factors arising from these other elements are based on Table 3.12 in the *SES Handbook*, as shown in Table A-2.

[11] See p. 5-16, Equation 5.37.

[12] See Fig. 5.3.

Table A-2. Friction Factors in Horseshoe Tunnels

	1-track	2-track	3-track
Width × Height, ft	17 × 17	34 × 17	51 × 25
Hydraulic diameter, D_H, ft	18.5	26	38
Relative roughness, k/D_H	0.00054	0.00038	0.00026
$f_{\text{wall surface}}$	0.017	0.016	0.015
$f_{\text{other elements}}$	0.01	0.01	0.01
f_{tunnel}	0.027	0.026	0.025

A.3 Cast-iron Tubes

Single-track, cast-iron tubes are used under rivers (e.g., Joralemon Tubes, Steinway Tubes). These are fabricated of 18-in. curved plates bolted to flanges, which result in an internal ribbing that dominates the friction factor. The tubes have an internal diameter of 15.5 ft between the 9-in. flanges, and therefore an outside diameter of 17 ft, as accounted for in Table A-3.

Table A-3. Friction Factors in Circular Cast-iron Tubes

Outside Diameter, ft	17
Flange Spacing, λ	1.5
λ/D	0.088
Relative roughness, k/D	0.00002
$f_{\text{wall surface}}$	0.009
f_{ribs}	0.04
f_{tunnel}	0.049

This page intentionally left blank.

Appendix B: Deposition Velocities in Subway Tunnels and Train Cars

B.1 Settling Velocity

For particles larger than about 2 μm, gravitational settling is usually the primary mechanism governing deposition. The settling velocity, V_g, is determined by a balance of the gravitational force and the particle drag (Hinds 1982[13]), such that:

$$V_g = \frac{d_p^2 \, \rho_p \, g \, C_c}{18 \, \mu},$$

where d_p is the particle diameter, ρ_p is the particle density, g is gravitational acceleration, μ is the dynamic viscosity of air, and C_c is the slip correction factor (Hinds 1982[14]):

$$C_c = 1 + \frac{\lambda}{d_p}\left(c_1 + c_2 \exp\left(-c_3 \frac{d_p}{\lambda}\right)\right),$$

with $c_1 = 2.514$, $c_2 = 0.80$, and $c_3 = 0.55$; λ is the mean free path for air ($\lambda = 0.066$ μm at 1 atm and 293 K), so that

$$\lambda = \frac{12 \, \mu \sqrt{\pi T}}{P},$$

where T is the absolute temperature, and P is the pressure.

B.2 Forced Convection

Deposition due to forced convection in a turbulent flow is calculated using empirical heat transfer relationships by invoking the Reynolds analogy for heat and mass transfer. According to the Reynolds analogy, because the turbulent fluxes of heat and mass arise from the same physical mechanism, the expressions for their turbulent diffusivities, which relate the fluxes to the mean advection, should have a similar form.

The empirically determined expression for the Nusselt number (the dimensionless heat transfer coefficient) in turbulent pipe flow is from Kays and Crawford (1980[15]):

[13] See page 45, Equation 3.21.

[14] See page 45, Equation 3.20.

[15] See page 245, Equation 13-10.

$$Nu = \frac{h\,D}{k_a} = \frac{f}{8}\,\frac{Re\,Pr}{1.07 + 12.7(Pr^{2/3} - 1)\sqrt{f/8}},$$

where h is the heat transfer coefficient; k_a is the thermal conductivity for air; D is the tunnel (hydraulic) diameter; Re is the Reynolds number; $Pr = \nu/\alpha$ is the Prandtl number, the ratio of kinematic viscosity ν to (molecular) thermal diffusivity α; and f is the Darcy-Weisbach friction factor discussed previously. By the Reynolds analogy, the corresponding expression for the Sherwood number, the dimensionless mass transfer coefficient, is:

$$Sh = \frac{V_{fc}D}{\mathscr{D}} = \frac{f}{8}\,\frac{Re\,Sc}{1.07 + 12.7(Sc^{2/3} - 1)\sqrt{f/8}},$$

where V_{fc} is the deposition velocity for forced convection, and $Sc = \nu/\mathscr{D}$ is the Schmidt number or the ratio of kinematic viscosity to the Brownian diffusion coefficient $\mathscr{D}$:

$$\mathscr{D} = \frac{\kappa\,T\,C_c}{3\,\pi\,\mu\,d_p},$$

κ is Boltzmann's constant, T is temperature, C_c is the slip correction factor, μ is the dynamic viscosity, and d_p is the particle diameter. Then, the deposition velocity is as follows:

$$V_{fc} = \frac{\mathscr{D}}{D}\,\frac{f}{8}\,\frac{Re\,Sc}{1.07 + 12.7(Sc^{2/3} - 1)\sqrt{f/8}};\ \begin{cases} 0.5 < Pr, Sc < 2000 \\ 10^4 < Re < 5 \times 10^6 \end{cases}.$$

For very large Schmidt numbers characteristic of particle diameters over 0.1 μm, this expression for V_{fc} may not be valid. However, Bejan et al. (2003) point out that this expression is valid for $Sc < 10^6$ if 10% errors are tolerable; accordingly, it is used in BGM for all particle sizes. Possibly substantial errors introduced for particle sizes > 5 μm are rendered negligible by gravitational settling, which dominates for these particle sizes.

B.3 Natural Convection

In the absence of forced convection due to the train-induced airflows, natural convection, which arises from thermal buoyancy, is important for both transport and deposition of material. In a subway system, natural convection flows can arise axially along the tunnels due to elevation and temperature differences, and vertically up or down tunnel walls. Axial transport from natural flows is included in the calculation of tunnel airflows, for which deposition will be calculated using the deposition velocity for forced convection. In this section, the vertical transport and deposition onto the walls, ceiling, and floor of the tunnel by natural convection are determined. As was the case for forced convection, the development of expressions for deposition velocity in natural convection flows utilizes empirical expressions developed for heat transfer. The heat transfer relationship for natural convection along a vertical surface from Nazaroff and Cass (1989) is:

$$Nu = \left(0.825 + \frac{0.387\ Ra^{1/6}}{[1 + (0.492/Pr)^{9/16}]^{8/27}}\right)^2,$$

and the Rayleigh number is

$$Ra = \frac{g\ \beta\ |T_w - T_a|\ D^3}{\nu\ \alpha},$$

where T_w and T_a are, respectively, the wall and air temperature, and β is the coefficient of thermal expansion:

$$\beta = -\frac{1}{\rho}\left(\frac{\partial \rho}{\partial T}\right)_P.$$

For an ideal gas such as air, $\beta = 1/T_a$.

By the Reynolds analogy, the deposition velocity from Nazaroff and Cass (1989) is:

$$V_{nc} = \frac{\mathscr{D}}{H}\left(0.825 + \frac{0.387\ Ra^{1/6}}{[1 + (0.492/Sc)^{9/16}]^{8/27}}\right)^2,$$

where H is the height of the tunnel. This expression is reportedly valid for $Ra < 10^{12}$ and for all Prandtl and Schmidt numbers (Gebhart et al. 1988). However, when used for mass transfer, it appears to provide somewhat different results from the relationship proposed by Nazaroff and Cass (1987) for mass transfer in laminar natural convection flows.

For the case where the floor of the tunnel is warmer than the air or the ceiling is cooler than the air, the deposition velocity is derived from the expression for heat transfer from a horizontal plate with the heated surface facing upward or the cooled surface facing downward (Kays and Crawford 1980[16]):

$$V_{nc} = \frac{\mathscr{D}}{W}\ 0.15\ Ra^{1/3},$$

where W is the tunnel width. This expression is valid from $10^5 < Ra < 10^{11}$. For the case where the ceiling is warmer than the air or the floor is cooler, the deposition velocity is set equal to the value for the walls because the airflow over that surface will be caused by natural convection along the tunnel walls.

For round tunnels, the diameter is substituted for the height and width.

[16] See page 328, Equation 16-33.

B.4 Thermophoretic Effects

Thermophoretic effects can be important if the tunnel wall temperature is substantially different from the tunnel air temperature. A cool tunnel wall coupled with warmer tunnel air will enhance deposition, whereas a warm tunnel wall coupled with cooler tunnel air will retard deposition. The relative importance of thermophoresis will depend on the temperature difference between the air and the wall; however, it is the temperature difference in the vicinity of the wall rather than any large-scale temperature difference that is important. For the sake of tractability, BGM adopts the approach of Nazaroff and Cass (1987) in addressing indoor deposition wherein thermophoretic effects are evaluated using the temperature difference between the wall and the core of the flow, although it may not be entirely appropriate for laminar flows where the temperature gradient near the wall may be small (e.g., natural convection flows).

The thermophoretic deposition velocity V_t from Nazaroff and Cass (1989) is:

$$V_t = -N_t \, Nu \, \frac{\nu}{D}.$$

The Nusselt number is selected for the particular flow regime (as described earlier for forced convection or natural convection), where N_t is a dimensionless thermophoretic parameter such that:

$$N_t = K_t \, \frac{T_w - T_a}{T_a},$$

and

$$K_t = 2 \, C_s \, \frac{\left(\frac{k_a}{k_p} + C_t \mathrm{Kn}\right)\left(1 + \mathrm{Kn}\left(1.2 + 0.41 \exp(-0.88 \, \mathrm{Kn})\right)\right)}{(1 + 3 \, C_m \mathrm{Kn})\left(1 + 2\frac{k_a}{k_p} + 2 C_t \mathrm{Kn}\right)}.$$

In this expression, k_a and k_p are the thermal conductivities of the air and particle, respectively; $Kn = 2\lambda/d_p$ is the Knudsen number; $C_m = 1.146$; $C_s = 1.147$; and $C_t = 2.20$.

B.5 Discussion

A comparison of deposition rates from settling, forced convection, and thermophoretic effects is presented in Figure B-1 for a typical subway tunnel ($D = 5$ m, $r = k/D = 0.005$, $T_a = 300$ K) with a tunnel airflow velocity of 10 m/s. For particles larger than 0.1 μm, thermophoretic effects dominate the effects of forced convection for even small air/wall temperature differences. This means that for the case where the air is cooler than the wall, little or no deposition will occur for particles less than about 1 μm given that thermophoretic deposition velocity is negative. It is also important to note that for particles larger than 0.5 μm, settling dominates the effects of forced convection; and for particles larger than 2 μm, settling dominates thermophoretic effects. Figure B-2 provides a similar comparison but for a tunnel air velocity of 1 m/s. In this case, thermophoretic effects also dominate forced convection for particles larger than 0.1 μm. However, the relative influence of settling is greatly increased because deposition due to forced convection and thermophoretic effects is substantially reduced.

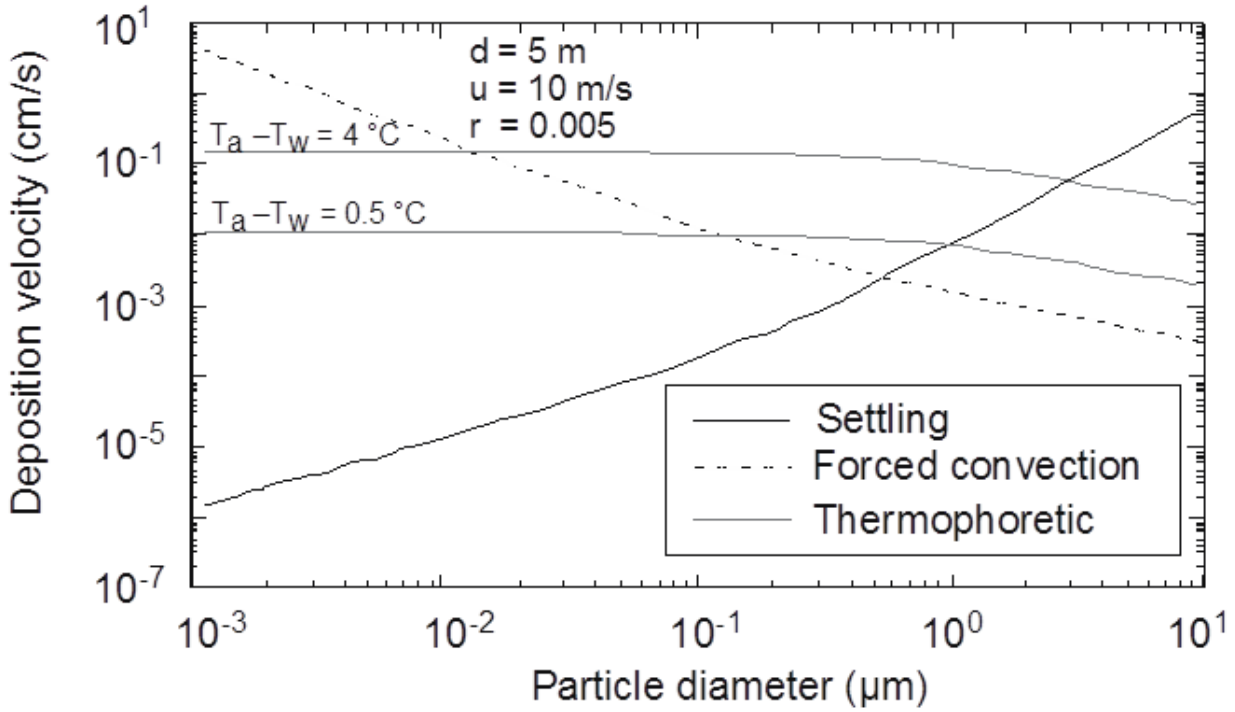

Figure B-1. Deposition velocity due to settling, forced convection, and thermophoretic effects for a typical subway tunnel and a tunnel airflow velocity of 10 m/s.

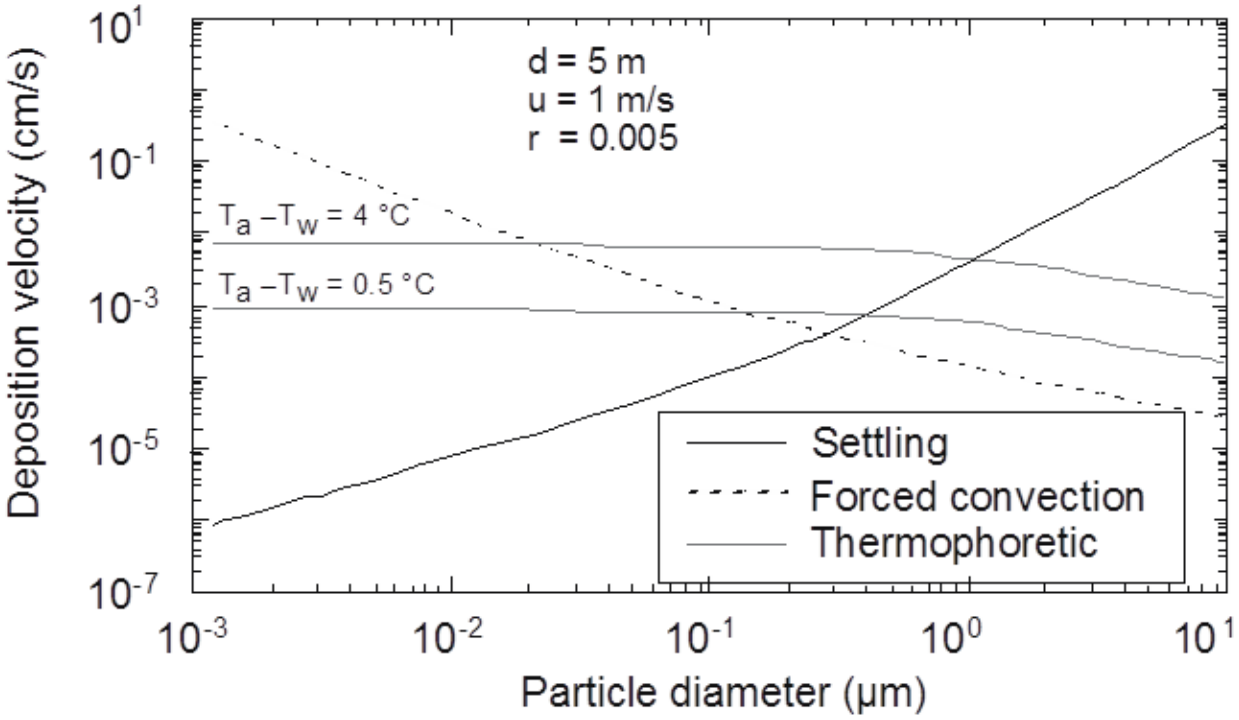

Figure B-2. Similar to Figure B-1 except for a tunnel airflow velocity of 1 m/s.

Appendix C: Determination of Sorption Rate Constants

As discussed in Section 6, the Argonne Below Ground Model (BGM) implements the "2-sink" model of Singer et al. (2005, 2007), in which airborne material is adsorbed by or desorbed from a surface layer, which, in turn, exchanges material by diffusion with a substrate layer that is not exposed to the air. These exchanges are described by the following set of equations[17]:

$$\frac{dC}{dt} = -\lambda_a C + \lambda_d \frac{m_1}{\tilde{V}}; \tag{C.1}$$

$$\frac{dm_1}{dt} = -(\lambda_d + k_1)m_1 + \lambda_a C\tilde{V} + k_2 m_2; \tag{C.2}$$

$$\frac{dm_2}{dt} = -k_2 m_2 + k_1 m_1. \tag{C.3}$$

Here, C is the airborne mass concentration; m_1 and m_2 are the masses contained in the surface and substrate layers, respectively; $\tilde{V}$ is the volume of the train car or tunnel/station segment; and λ_a, λ_d, k_1, and k_2 are the rate constants for adsorption by the surface, desorption from the surface, diffusion from the surface to the substrate, and diffusion from the substrate to the surface, respectively.

This model may be related to the "1-sink" model described by Karlsson and Huber (1996) by setting $k_1 = k_2 = 0$. Karlsson and Huber present Equation C.1 in terms of the net surface adsorption:

$$\frac{dC}{dt} = -\frac{S}{\tilde{V}} a(C - C_1). \tag{C.4}$$

Here, S is the area of the adsorbing surface, C_1 is the concentration at the surface, and a is a proportionality constant with units of velocity (analogous to a deposition velocity). The concentration at the surface is posited to be proportional to the surface loading, $C_1 = b\, m_1/S$; b is a proportionality constant with units of inverse length. Substituting this expression into Equation C.4 yields

$$\frac{dC}{dt} = -\frac{S}{\tilde{V}} a\left(C - b\frac{m_1}{S}\right) = -\frac{S}{\tilde{V}} aC + ab\frac{m_1}{\tilde{V}}. \tag{C.5}$$

Comparing Equations C.1 and C.5, it is apparent that

$$\lambda_a = aS/\tilde{V}, \tag{C.6a}$$

and

$$\lambda_d = ab. \tag{C.6b}$$

[17] Equations C.2 and C.3 are expressed in terms of mass whereas Singer presented them in terms of concentration, $m/\tilde{V}$, to be consistent with Equation C.1. The rate constants are the same in either form.

Equation C.6a indicates that λ_a is proportional to the surface-area-to-volume ratio $S/\tilde{V}$. Singer et al. (2007) found no correlation between λ_a and $S/\tilde{V}$ in his experiments conducted in 10 residential rooms, for which $S/\tilde{V}$ varied from 2.9 to 4.6 m^{-1}. However, in Singer et al.'s (2007) study, the rooms with the largest values of $S/\tilde{V}$ were bathrooms with a large proportion of hard surfaces (e.g., tile) for which a would likely be lower than it would be for a carpeted surface, furnished rooms that had smaller values of $S/\tilde{V}$, thereby possibly obscuring the correlation between λ_a and $S/\tilde{V}$. For a typical two-track subway tunnel, $S/\tilde{V} \approx 0.75$ m^{-1}, and for a typical station, $S/\tilde{V} \approx 0.2$ m^{-1}, which suggests that the relationship between λ_a and $S/\tilde{V}$ expressed in Equation C.6a needs to be included to produce realistic adsorption rates in the subway.

Singer et al. (2007) determined values for the rate constants for both one-sink and two-sink models using a range of chemicals including organophosphate (OP) surrogates for G-series nerve agents based on experiments in actual residential settings and in a laboratory chamber furnished to represent a residential setting. Singer et al.'s (2007) chamber results are presented in Table C-1. Values for the rate constants λ_a and λ_d derived from Karlsson and Huber (1996) using Equations C.6a and C.6b are presented in Table C-2.

Table C-1. Rate constants for a furnished chamber (Source: Singer et al. 2007, Table 5).

Chemical	Model	λ_a (h^{-1})	λ_d (h^{-1})	k_1 (h^{-1})	k_2 (h^{-1})
DMMP[a]	1-sink	2.5	0.08	–	–
	2-sink	4.3	0.86	0.54	0.08
DEEP	1-sink	3.2	0.13	–	–
	2-sink	5.0	0.79	0.42	0.10
TEP	1-sink	3.8	0.13	–	–
	2-sink	5.6	0.75	0.43	0.11

[a] DMMP = di-methyl methylphosphonate; DEEP = diethyl ethyl-phosphonate; TEP = triethylphosphate.

Table C-2. Rate constants for the 1-sink model derived from Karlsson and Huber (1996).

Chemical	S/V (m^{-1})	a (m s^{-1})	b (m^{-1})	λ_a (h^{-1})	λ_d (h^{-1})
GB to wallpaper	5.8	1.7×10^{-4}	0.45	3.5	0.28
GB to rough spruce	6.4	1.3×10^{-4}	0.73	3.0	0.34
GB to unpainted concrete	2.2	7.2×10^{-4}	0.026	5.7	0.067
GB to textile	—	2.4×10^{-4}	0.094	—	0.081
VX to painted walls	3.5	2.5×10^{-4}	0.07	3.2	0.063

For the one-sink model, the rate constants λ_a and λ_d for the OPs were in reasonably good agreement with values derived from Karlsson and Huber's results for similar surfaces. However, Karlsson and Huber's (1996) results for GB adsorption to unpainted concrete yielded a significantly larger value for λ_a than Singer et al.'s (2007) experiments for residential settings. Accordingly, for the subway we use Karlsson and Huber's (1996) value for a for GB adsorption to unpainted concrete[18] combined with the appropriate $S/\tilde{V}$ according to Equation C.6a to determine λ_a. For sorption to subway patrons' clothing, we use Karlsson and Huber's (1996) value for a for GB adsorption to "textile."

Singer et al. (2007) pointed out that for the two-sink model, the rate constant k_2 that controls diffusion from the substrate to the surface actually controls the overall desorption (because it is the smallest rate) and has values nearly equal to λ_d for the one-sink model. Because Singer et al.'s (2007) values for k_2 were in reasonable agreement with the values of λ_d derived from Karlsson and Huber's results for desorption of GB from concrete and textiles, and because values for λ_d, k_1, and k_2 determined for the OPs from the chamber tests showed little variation, we have implemented the values for DMMP as reported by Singer et al. (2007).

[18] Karlsson and Huber's (1996) results for unpainted concrete were obtained from laboratory results using concrete samples prepared for that purpose and "aged" by heating. Recent work by Massachusetts Institute of Technology Lincoln Laboratory (Ervin 2013) using concrete samples taken from actual subway platforms reveals a much smaller rate of adsorption of OP surrogates, attributed to "grime" filling the pores of the concrete. This finding suggests that Karlsson and Huber's results may not be applicable to subways.

Decision and Information Sciences Division
Argonne National Laboratory
9700 South Cass Avenue, Bldg. 221
Argonne, IL 60439-4844

www.anl.gov